Explaining the Equatorial Pacific Thermocline Response to Climate Change with a Model Hierarchy

Matthew T. Luongo[1,2*], Shang-Ping Xie[3], Ian Eisenman[3], Shantong Sun[4], & Kyle Armour[2,5]

1. Cooperative Institute for Climate, Ocean, & Ecosystem Studies, University of Washington, Seattle, WA, USA
2. School of Oceanography, University of Washington, Seattle, WA, USA
3. Scripps Institution of Oceanography, UC San Diego, La Jolla, CA, USA
4. Laoshan Laboratory, Qingdao, China
5. Department of Atmospheric & Climate Science, University of Washington, Seattle, WA, USA

* mluongo@uw.edu

This manuscript is a pre-print submitted to EarthArXiv.

The pre-print has been submitted for review to *Journal of Geophysical Research: Oceans*.

Subsequent versions may have altered content.

Explaining the Equatorial Pacific Thermocline Response to Climate Change with a Model Hierarchy

Matthew T. Luongo[1,2], Shang-Ping Xie[3], Ian Eisenman[3], Shantong Sun[4], & Kyle C. Armour[2,5]

[1]Cooperative Institute for Climate, Ocean, & Ecosystem Studies, University of Washington, Seattle, WA
[2]School of Oceanography, University of Washington, Seattle, WA
[3]Scripps Institution of Oceanography, UC San Diego, La Jolla, CA
[4]Laoshan Laboratory, Qingdao, China
[5]Department of Atmospheric & Climate Science, University of Washington, Seattle, WA

Key Points:

- Climate models can largely recreate observed equatorial Pacific subsurface temperature trends from 1958-2020
- The observed subsurface temperature change is due to wind changes, remote SST changes, and local SST changes
- Our results suggest that canonical drivers of the equatorial Pacific response to climate change have been misattributed

Corresponding author: M.T. Luongo, mluongo@uw.edu

Abstract

Most studies of the equatorial Pacific response to anthropogenic forcing have focused on patterns of sea surface temperature (SST) change. However, similar SST patterns can be consistent with a range of different subsurface responses, each with differing physical and biogeochemical implications. While historical observation and climate model mismatches have been suggested in the literature, we show that model simulations can largely capture the observed 1958-2020 subsurface temperature trend in the equatorial thermocline. We then analyze a hierarchy of idealized model simulations, consisting of fully-coupled, mechanically-decoupled, ocean-only, and reduced gravity models, to understand which ocean dynamics contribute to this response. We show that the response of the thermocline to idealized climate change can be explained by a combination of decadal Bjerknes-like momentum dynamics and radiatively-forced buoyancy-driven dynamics. We further decompose the buoyancy-driven pattern into a pattern driven by remote, subtropical SST forcing and a pattern driven by local, equatorial SST forcing. The remote-SST-forced pattern of thermocline warming shows the signature of dynamic and thermodynamic subtropical cell adjustments. Meanwhile, increased stratification in the local-SST-forced pattern both coherently shoals the thermocline and relaxes thermocline tilt to largely cool the thermocline. Considered together, we recreate the long-term subsurface equatorial Pacific response to idealized greenhouse gas forcing as a linear combination of (i) wind-stress-driven changes, (ii) remote buoyancy-driven changes, and (iii) local buoyancy-driven changes. To conclude we discuss implications for recent temperature trends, revisit canonical theories of the ocean dynamical thermostat, and show the insensitivity of forced responses to forcing geography.

Plain Language Summary

While most research on the equatorial Pacific response to climate change has focused on surface ocean temperatures, ocean circulation changes provide insight into the dynamic drivers of that response. For instance, though eastern equatorial Pacific surface cooling could result from either strengthening winds or subsurface communication of subtropical cooling, these mechanisms affect the subsurface distinctly. In this work we first show that climate model simulations can largely capture the observed 1958-2020 equatorial Pacific subsurface temperature response to climate change. We then use a series of idealized modeling simulations, from a complex global climate model to a sim-

ple primitive equation model, to explain the ocean dynamics that create this response. Our central result is that the equatorial Pacific subsurface temperature response to climate change is a simple linear sum of the ocean's response to changes in winds, changes in remote sea surface temperature patterns, and changes in local sea surface temperature patterns. We explore the dynamics of each of these individual responses. Last, we show that this understanding does not explain subsurface temperature patterns since the late 1970s, and we discuss how our results suggest a reinterpretation of how certain ocean dynamics shape the equatorial ocean's response to climate change.

1 Introduction

A strong zonal gradient in sea surface temperature (SST) exists in the equatorial Pacific between the western Pacific warm pool and the eastern Pacific cold tongue. This zonal SST gradient is the most obvious manifestation of a series of coupled atmospheric and oceanic processes that connect easterly trade winds, westward surface currents, an eastward subsurface return flow within an upward tilting thermocline, and upwelling of cool sub-thermocline waters in the eastern equatorial Pacific (Bjerknes, 1969; Wyrtki, 1975). Variability in the equatorial Pacific mean state shifts the location of atmospheric deep convection and excites planetary waves that propagate to the extratropics to affect global climate (Horel & Wallace, 1981). Across a broad range of time-scales, from interannual changes of the El Niño-Southern Oscillation (ENSO, Philander, 1983) to decadal changes of the Pacific Decadal Oscillation (PDO, Mantua et al., 1997), the equatorial Pacific is a key driver and pacemaker for global climate (e.g., Kosaka & Xie, 2016).

Given its outsize influence on Earth's climate, it is critical to understand how the equatorial Pacific will respond to anthropogenic greenhouse gas emissions (e.g., DiNezio et al., 2009; Xie et al., 2010). A key question, which has received much attention and debate, is: How will the equatorial zonal SST gradient change in the future? Constraints from atmospheric thermodynamics have been primarily invoked in support of a decreasing gradient (i.e., more warming in the eastern than western equatorial Pacific): enhanced evaporative cooling in the warmer western Pacific can more readily balance anomalous radiative forcing than the cooler eastern Pacific (Knutson & Manabe, 1995; Merlis & Schneider, 2011), and the atmospheric Walker circulation slow-down implied by specific humidity changes would relax thermocline tilt (Vecchi & Soden, 2007). Meanwhile, Clement et al. (1996) and Seager and Murtugudde (1997) proposed the "ocean dynamical ther-

mostat" and suggested that the zonal SST gradient should in fact increase. The thermostat theory suggests that the eastern equatorial Pacific should warm by less than the rest of the tropics because upwelled equatorial waters, originating in the extratropics and reaching the equator via the oceanic subtropical cells (STCs: Liu, 1994; McCreary Jr & Lu, 1994), will not show an effect of surface forcing until some time later. More recently, several studies have suggested that this debate is simply a matter of time-scales, with a brief strengthening of the zonal gradient eventually giving way to a long-term weakening (Luo et al., 2017; Heede et al., 2020, 2021; Heede & Fedorov, 2021).

However, the continued inability of coupled models to recreate recent historical equatorial Pacific SST trends (Coats & Karnauskas, 2017; Seager et al., 2019, 2022; Watanabe et al., 2021; Wills et al., 2022) calls into question this seeming resolution. While observational products suggest that the western Pacific has warmed and central-eastern Equatorial Pacific has cooled since the beginning of the satellite era (e.g., Karnauskas et al., 2009; Solomon & Newman, 2012; Seager et al., 2019; Wills et al., 2022), over that same period the vast majority of coupled global climate models (GCMs) show enhanced warming in the eastern Pacific relative to the western Pacific. Many studies have attempted to explain the mismatch between observed and modeled equatorial Pacific SST trends, pointing to i) mismatched internal variability (e.g., Laepple & Huybers, 2014; Olonscheck et al., 2020; Watanabe et al., 2021; Heede & Fedorov, 2023; Jiang et al., 2024a), ii) incorrect model processes that could otherwise create observed trends (e.g., McGregor et al., 2018; Baldwin et al., 2021; Dong et al., 2022; Kang et al., 2023; Hwang et al., 2024), and iii) systematic biases in model mean states that do not allow a forced response to establish (Seager et al., 2019, 2022; Heede & Fedorov, 2023; Jiang et al., 2024a, 2025).

While the mismatch between observed and modeled historical equatorial SST has been extensively discussed, the subsurface equatorial temperature response to climate change has been relatively understudied. This top-down focus on SST alone potentially obfuscates important subsurface oceanic adjustments (e.g., Clement et al., 1996; Vecchi & Soden, 2007) that have helped to shape the SST response. For instance, despite comprising entirely different subsurface dynamics, both decreased thermocline tilt (Vecchi & Soden, 2007; Luongo et al., 2023) and coherent thermocline deepening (Luongo et al., 2025) could theoretically lead to an El Niño-like SST pattern.

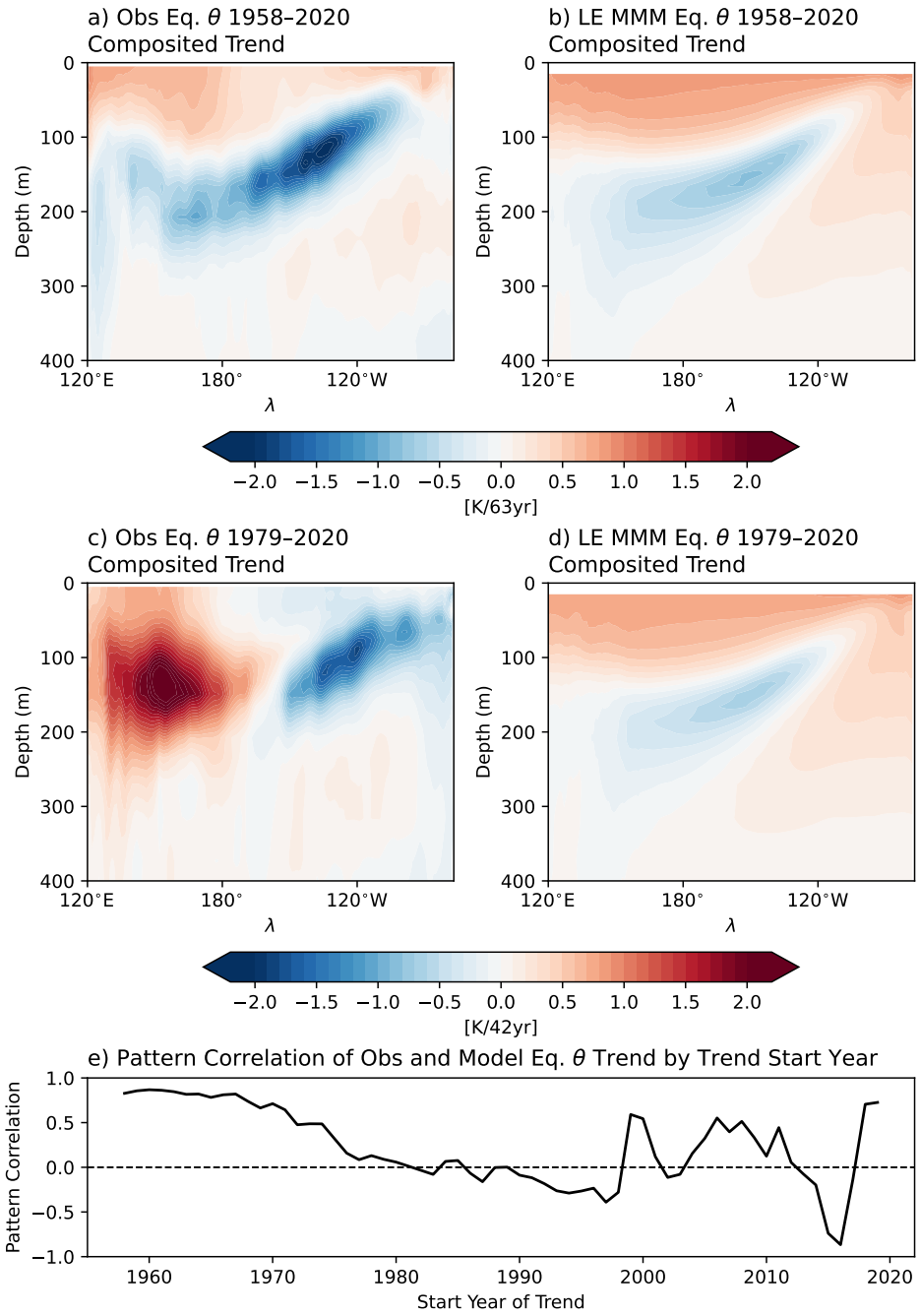

Figure 1. a) 1958-2020 annual-mean equatorial temperature (θ) trend composited from EN04 and Ishii observational products and ORAS5 and SODA2.2.4 reanalyses. b) Multi-model mean equatorial θ from 11 large ensemble simulations over 1958-2020. c) As in panel a) but for the period of 1979-2020. d) As in panel b) but for the period of 1979-2020. e) Pearson pattern correlation between observational and multi-model mean equatorial θ trend as a function of trend start year.

Following Jiang et al. (2025), we show a composite of the 1958-2020 subsurface equatorial (meridionally averaged from 5°S-5°N) Pacific temperature trend from two observational products [EN04 (1958-2020, Good et al., 2013) & Ishii (1958-2012, Ishii & Kimoto, 2009)] and two ocean reanalyses [ORAS5 (1958-2020, Zuo et al., 2019) & SODA2.2.4 (1958-2010, Carton & Giese, 2008)] (Figure 1a). The most obvious feature of subsurface equatorial temperatures over the past 60 years is a broad thermocline cooling. Due to the upward and eastward tilt of the thermocline, this cooling is around 250m deep in the west-central Pacific and around 50m deep in the eastern Pacific. Maximum cooling occurs between 150°W-120°W from approximately 100-175m. While the cooling is the most eye-catching feature in this observational pattern, we also note a broad surface warming, which is minimized in the central Pacific and extends deeper in the western Pacific than eastern Pacific, and a sub-thermocline warming in the eastern Pacific. These features are largely shared by individual observational products (Figure S1).

The observed 1958-2020 subsurface temperature trend in Figure 1a is similar to the 1951-2010 trend pattern in Watanabe et al. (2021). We note, however, that the specific time period considered greatly influences this pattern: Figure 1a is markedly different than both the 1979-2020 pattern (Figure 1c) and the 1979-2013 pattern (Watanabe et al., 2024). The observed trend over this shorter period features a striking zonal temperature dipole, western Pacific warming and the eastern Pacific cooling, within the top 200m. This temperature dipole dynamically agrees with the upper ocean circulation strengthening noted by Tuchen et al. (2024) over the overlapping period of 1993-2022.

In a series of recent studies inspired by Seager et al. (2019)'s hypothesis that the models' mean state ocean is simply too biased to capture observed SST trends, Jiang et al. (2024a, 2024b, 2025) highlight the differences in the subsurface trend patterns between observations and models. In particular, the authors hypothesize that the observed subsurface cooling response can be explained as a forced response to wind changes (Jiang et al., 2024a, 2024b) and that models lack an effective connectivity between subsurface and surface eastern Pacific temperatures due to insufficient upwelling and mixing (Jiang et al., 2025). However, the corresponding 1958-2020 subsurface temperature trend composite from a suite of 11 large ensemble simulations from the sixth coupled model intercomparison project [Figure 1b, inspired by Jiang et al. (2025)] shows a similar pattern to observations (Figure 1a; Pearson pattern correlation of 0.83). Both show a broad thermocline cooling, a somewhat zonally symmetric surface warming, and a sub-thermocline

eastern Pacific warming. Indeed, despite model biases, there is general agreement between observed and modeled subsurface temperature trends when those trends begin before ∼1975 (Figure 1e), suggesting that the modeled subsurface temperature trend can still inform our understanding of the observed subsurface temperature trend and the coupled dynamics that have created it. This perspective motivates the central questions of our study: 1) which ocean dynamics contribute to this common modeled response, and 2) to what extent is the full response a simple linear combination of these responses?

A handful of studies have explored the models' shared central-western Pacific thermocline cooling response (c.f. Figure 1b and Figure S2) which has persisted for several model generations. Vecchi and Soden (2007) suggest that this cooling is a local effect caused by a reduction in thermocline tilt due to a weaker atmospheric Walker circulation. Yang et al. (2009) suggest that this weaker Walker circulation slows down the STCs and dynamically cools the equatorial subsurface. Luo et al. (2009, 2018) agree that models' STCs have slowed, but suggest that a major cause of the slowdown is increased subtropical surface stratification. Finally, Ju et al. (2022) suggest that the cooling is caused by mean advection of density-compensated spiciness anomalies from the subtropics, which cool the region as much as dynamical changes in subtropical cell circulation.

While these studies provide a starting point for answering our guiding questions, it's evident that these proposed mechanisms are entwined with murky causality. A common means of circumventing the attribution issues common to coupled dynamics is to employ a model hierarchy to step through a complex response by iteratively removing complexity until the phenomenon of interest is isolated. For instance, recent studies have overrode surface wind stress to mechanically decouple a GCM's ocean from its atmosphere (e.g., Luongo et al., 2024) and have shown that the ocean's full response to an anomalous forcing can be linearly partitioned into the response due to anomalous surface buoyancy forcing and anomalous surface momentum forcing (Luongo et al., 2022, 2023). Similarly, ocean-only GCM (OGCM) simulations are a convenient way to isolate just the ocean's response to a forcing without changes in the atmosphere (e.g., Peng et al., 2022).

In this study we employ a model hierarchy, consisting of a fully-coupled GCM, a mechanically-decoupled GCM, an OGCM, and a primitive equation reduced gravity model, to explore the modeled subsurface equatorial Pacific temperature response to greenhouse gas forcing and which ocean dynamics contribute to it. We discuss the simulations that

comprise this hierarchy in section 2 and in section 3 we show that the full response can be understood as a linear sum of the response due to i) momentum effects, ii) remote buoyancy effects, and iii) local buoyancy effects. We discuss implications of these results in section 4 and we conclude in section 5.

2 Model Hierarchy

All simulations used to explore the equatorial Pacific thermocline response to greenhouse gas forcing are presented in Table 1. Simulations that explore the equatorial Pacific thermocline response to non-greenhouse-gas forcing schemes are presented in Table S1.

2.1 Fully-Coupled Simulations

We analyze pre-existing simulations using the National Center for Atmospheric Research's Community Earth System Model, Version 1.2 (CESM1: Hurrell et al., 2013) that were initially presented in Luongo et al. (2022) and Taylor et al. (2025). These simulations have a nominal horizontal resolution of 2° in the atmosphere and land components and 1° in the ocean and sea ice components, though the oceanic component has higher resolution near the equator to better resolve equatorial dynamics. They are run in a standard coupled configuration with pre-industrial forcing ("B1850" compset) for fifty years.

Our preindustrial control (Ctrl) simulation extends directly from initialization with no anomalous forcing applied. To idealize climate change we apply and maintain an abrupt quadrupling of CO_2 relative to pre-industrial levels (CO_2x4). While abrupt quadrupling of CO_2 is an obvious simplification compared to a more realistic time-evolving increase in CO_2, we show in section 3.1 that this idealization works remarkably well. While we primarily focus on the equatorial Pacific's response to greenhouse gas forcing in this study, we also consider simulations with hemispherically asymmetric forcing to test how robust the ocean dynamics of interest are to forcing geometry. We apply a zonally-uniform top-of-atmosphere (TOA) insolation reduction following the Extratropical-Tropical Interaction Model Intercomparison Project (ETINMIP: Kang et al., 2019) protocol in the Northern Hemisphere (NH, 45°N-65°N) for ETINMIPNH and in the Southern Hemisphere (SH, 45°S-65°S) for ETINMIPSH. The ETINMIP forcing corresponds to an annual-mean, zonal-mean forcing of approximately -45 Wm^{-2} at 55° N or S and falls off as an approximate

Fully-coupled Simulations		
Simulation Name	**CO_2 Forcing**	**Wind Stress**
Ctrl	280ppm	Freely evolving
CO_2x4	1120ppm	Freely evolving
Mechanically-decoupled Simulations		
Simulation Name	**CO_2 Forcing**	**Wind Stress**
Tau1CO_2x1	280ppm	Ctrl
Tau1CO_2x4	1120ppm	Ctrl
Tau4CO_2x1	280ppm	CO_2x4
Ocean-only Simulations		
Simulation Name	**SST Forcing Perturbation**	**SST Forcing Bounds**
OCtrl	n/a	n/a
CO_2x4_BFsst	Tau1CO_2x4-Tau1CO_2x1	90°S-90°N
CO_2x4_BFsstET	Tau1CO_2x4-Tau1CO_2x1	90°S-6°S, 6°N-90°N
CO_2x4_BFsstEQ	Tau1CO_2x4-Tau1CO_2x1	10°S-10°N
NEPac2CWarm	+2°C	147°W-123°W, 22°N-32°N
Reduced Gravity Simulations		
Simulation Name	**Reduced Gravity**	
RGCtrl	1x	
RGx2	2x	

Table 1. Details of the fully coupled, mechanically-decoupled, ocean-only, and reduced-gravity simulations used to study the equatorial Pacific thermocline response to greenhouse gas forcing. Table S1 presents simulations that explore alternate forcing schemes.

Gaussian. For all CESM1 simulations we consider an average over years 11-50 after the forcing is applied as in Luongo et al. (2022, 2023).

2.2 Mechanically-Decoupled Simulations

We perform wind stress overriding simulations (e.g., Luongo et al., 2024) to isolate the dynamic effect of buoyancy and momentum flux anomalies on the ocean, while still maintaining some amount of realistic atmosphere-ocean coupling. In a fully-coupled simulation the coupler interactively provides the ocean component with atmospheric wind stress. This momentum flux coupling then drives changes in the ocean state (e.g., equatorial thermocline tilt which changes the zonal SST gradient), which can then feed back on the atmosphere in the next coupling step (e.g., Bjerknes feedback). In wind stress overriding simulations, however, the GCM is instead modified to receive a known surface wind stress field, disabling the interactive coupling of momentum fluxes and mechanically decoupling the ocean from the atmosphere. All other coupling, including the effect of wind speed on turbulent heat fluxes, remain in tact.

In our mechanically-decoupled simulations we either apply a radiative forcing (CO_2 quadrupling or ETINMIP TOA forcing) and lock to Ctrl's wind stress field, or we apply no radiative forcing but we lock to a perturbed simulation's wind stress field. For example, we perform a simulation where we abruptly quadruple CO_2, but we override with unperturbed Ctrl wind stress (Tau1CO_2x4). This simulation highlights the radiatively-driven climate response because wind stress is unperturbed. We also perform a simulation where we apply no CO_2 forcing, but we override with the perturbed wind stress field from CO_2x4 to highlight the climate response just due to wind stress (Tau4CO_2x1). Similarly, we perform a simulation where we apply a reduction in insolation in the NH following the ETINMIP protocol described above, but we override with unperturbed Ctrl wind stress (Tau_1_S_NH), and we perform a simulation where we apply no insolation reduction, but we override with the perturbed wind stress field from ETINMIPNH (Tau_NH_S_1). Tau_1_S_SH and Tau_SH_S_1 are similar, but correspond to the SH ETINMIP simulations.

In these wind overriding simulations we prescribe the full interannually-varying wind stress field to maintain the impact of high-frequency mechanical variability on the surface ocean and reduce mean state biases (Luongo et al., 2024). Finally, in order to remove mean state biases introduced by the mechanical decoupling technique, we compare

these perturbed mechanically-decoupled simulations to a control mechanically-decoupled simulation (Tau1CO_2x1), which has no radiative forcing and wind stress locked to Ctrl. As such, our buoyancy-forced (BF) response is Tau1CO_2x4-Tau1CO_2x1 and our momentum-forced (MF) response is Tau4CO_2x1-Tau1CO_2x1. See discussion in Luongo et al. (2022, 2023, 2024) for more detail on this protocol.

2.3 Ocean-only Simulations

We use an ocean-only version of the Massachusetts Institute of Technology General Circulation Model (MITgcm) in the same configuration used in Luongo et al. (2025), which is similar to the Estimated the Circulation and Climate of the Ocean version 4 release 4 (ECCOv4r4: Forget et al., 2015) configuration. This OGCM has 1° horizontal resolution in the zonal direction and 1/3° meridional resolution at high and low latitudes (telescoping to 1° in midlatitudes). While not fully permitting high latitude mesoscale eddies, the higher resolution in the equatorial region begins to resolve equatorial waves and thus decrease tropical biases. This MITgcm configuration is forced with monthly climatologies of net air-sea fluxes of heat, freshwater, shortwave radiation, and zonal and meridional momentum diagnosed by Peng et al. (2022) from a 25-year control integration of ECCOv4r4 with bulk formulae forcing. In addition to climatological flux forcing, we restore SST and sea surface salinity to Peng et al. (2022)'s climatologies on a 10-day timescale. All of our OGCM simulations branch from a 100-year spin-up, at which point the upper-ocean is approximately equilibrated. See Luongo et al. (2025) for further details.

Our OGCM control simulation (OCtrl) is integrated for 30 years. We also perform a series of perturbation experiments where we add the anomalies in the BF SST field diagnosed from our mechanically-decoupled CESM1 simulations to the SST relaxation field. We add anomalies in the quasi-equilibrium (average over years 11-50) SST field calculated from Tau1CO_2x4-Tau1CO_2x1, Tau_1_S_NH-Tau1CO_2x1, and Tau_1_S_SH-Tau1CO_2x1 (producing ocean-only simulations CO_2x4_BFsst, ETINMIPNH_BFsst, and ETINMIPSH_BFsst, respectively). Comparing these SST-forced perturbation experiments with OCtrl shows the ocean-only dynamic response to the buoyancy-driven SST response. Because any temperature response within the first few depth levels is more likely to be driven by the strong surface relaxation than by a dynamical adjustment, we focus our discussion of the dynamics revealed by the OGCM simulations on the thermocline and below.

Finally, we split these perturbation experiments geographically into SST forcing from only the extratropical regions and SST forcing from only the equatorial region ("ET" or "EQ" appended to above names). In the extratropical SST forcing experiment we apply the full CESM1 buoyancy-driven SST anomaly field from 90°S-11°S and 11°N-90°N. We linearly taper this forcing to zero over 5° to 6°S and 6°N to avoid artificially large meridional forcing gradients. There is no anomalous SST forcing from 5°S-5°N in the extratropical SST forcing experiment. Similarly, in the equatorial SST forcing experiment we apply the full CESM1 buoyancy-driven SST anomaly field from 5°S-5°N, create a 5° linear taper to 10°S and 10°N, and do not anomalously force SST anywhere else. While we somewhat arbitrarily chose these meridional boundaries, we have found that using 10°S and 10°N for the full forcing bounds of the equatorial SST forced simulation (and changing other bounds accordingly) leads to small differences that do not affect our conclusions (not shown). Last, as a point of comparison with the extratropical SST forcing simulation described above, we consider the NEPac2CWarm simulation originally presented in Luongo et al. (2025), where a rectangular patch of +2°C SST warming is applied off the coast of California. For all OGCM simulations we consider the average over years 11-30 after the forcing is applied as in Luongo et al. (2025).

2.4 Reduced Gravity Simulations

Finally, we run two simulations using the 1.5-layer reduced gravity (RG) model to represent an idealization of the upper ocean's response to an increase in surface stratification. The set-up is borrowed directly from Sun and Thompson (2020), with geography consisting of three idealized ocean basins representing the Atlantic, Indian, and Pacific oceans and a zonally re-entrant channel representing the Southern Ocean from 45°S to the southern boundary. The total width is 220° and the latitudinal extent is from 72°S-72°N. The model solves for upper layer thickness, approximating thermocline depth, and has a 1° horizontal spacing. Sun and Thompson (2020) provide further details on this model.

We run two reduced gravity simulations. The first is a control simulation using standard parameters from Sun and Thompson (2020) (RGCtrl). The second branches from the tenth year of RGCtrl and instantaneously doubles the reduced gravity parameter to represent a stratification increase in response to climate change forcing (RGx2). We compare the difference between these two simulations ten years after that branch point.

3 Results

3.1 Buoyancy and Momentum Dynamics Create the Full Response

Despite the fact that our CESM1 simulations idealize climate change as an abrupt quadrupling of CO_2, the upper-ocean quasi-steady fully-coupled (FC) response (Figure 2a) bears a striking resemblance to the multi-ensemble mean response to realistic historical forcing in Figure 1b (Pearson pattern correlation of 0.94). As in the multi-model response, the FC equatorial temperature response features a thermocline cooling in the central Pacific, a strong surface warming that is deeper in the western Pacific than the eastern Pacific, and a sub-thermocline warming in the eastern Pacific. Luo et al. (2018) show a very similar CESM1 response to abrupt quadrupling of CO_2 (over years 41-90), which in turn also resembles the transient response (years 1-10) to this same forcing in two prior versions of CESM (Heede et al., 2021). It is interesting that the equatorial Pacific's subsurface temperature response to abrupt idealized climate change matches the response pattern to historical forcing so well, particularly since Heede et al. (2021) showed that the prominent thermocline cooling response to abrupt quadrupling disappears after 200 years and is instead replaced by a near-zero temperature response. While the centennial response to abrupt 4xCO_2 forcing is an unrealistic analog for transient climate change, the multi-decadal response to abrupt 4xCO_2 forcing shown in Figure 2a appears to be an appropriate tool for studying the multi-model response to greenhouse warming.

As in Luongo et al. (2023), who instead consider the subsurface equatorial temperature response to NH ETINMIP forcing, we find that the FC equatorial temperature response to CO_2 forcing (Figure 2a) is highly linear. That is, the fully-coupled (FC) response to CO_2 forcing can be neatly linearly decomposed into the buoyancy-forced (BF) response (Figure 2b) and the momentum-forced (MF) response (Figure 2c):

$$\mathrm{FC} \approx \mathrm{BF} + \mathrm{MF} \ . \tag{1}$$

Comparing Figure 2a with the sum of Figures 2b & c explicitly shows this linearity (Figure S3a). These patterns closely resemble the FC, BF, and MF responses to NH ETINMIP forcing (but with opposite sign because ETINMIP forcing is a cooling) presented in Luongo et al. (2023) and recreated in Figures S4a-c. This resemblance is also found

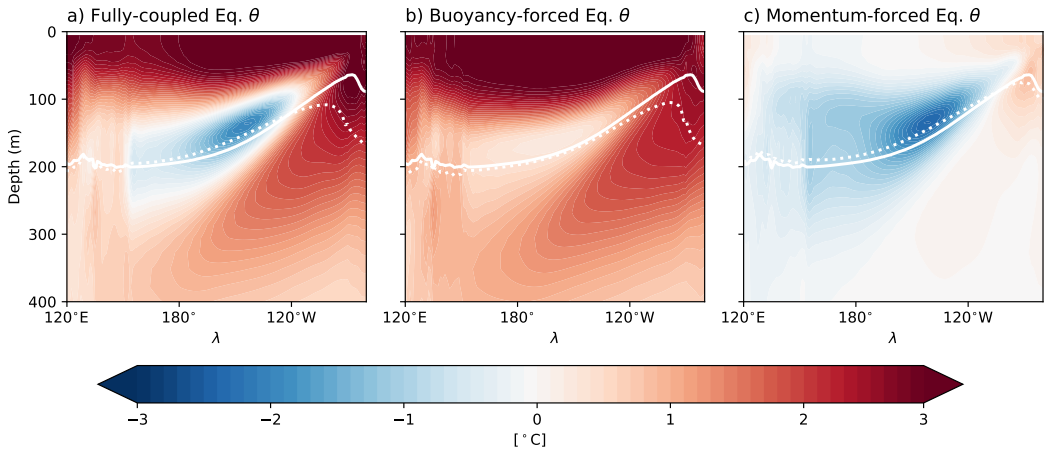

Figure 2. a) CESM1 fully-coupled (FC = CO_2x4-Ctrl) equatorial temperature (θ) response to abrupt quadrupling of CO_2. b) CESM1 buoyancy-forced (BF = Tau1CO_2x4-Tau1CO_2x1) equatorial θ response to abrupt quadrupling of CO_2. c) CESM1 momentum-forced (MF = Tau4CO_2x1-Tau1CO_2x1) equatorial θ response to abrupt quadrupling of CO_2. All panels are meridionally averaged from 5°S-5°N and temporally averaged from years 11-50. The 16°C isotherm from Ctrl is plotted as a solid white contour in all three panels and approximates the mean thermocline. Dotted white contours are the 16°C isotherm in the forced experiments: a) CO_2x4, b) Tau1CO_2x4, and c) Tau4CO_2x1.

in response to SH ETINMIP forcing (Figure S4d-f). This similarity between equatorial temperature responses was not expected a priori because abrupt 4xCO_2 is a nearly hemispherically symmetric forcing while ETINMIP forcing is purposefully hemispherically asymmetric. We discuss this further in Section 4.

The MF response, created by momentum-driven dynamics, is the cause of the prominent thermocline cooling seen in the FC response, qualitatively agreeing with Jiang et al. (2024b, 2025)'s assertion that winds have driven much of the observed subsurface equatorial temperature response. This cooling is maximized within the thermocline and is a major feature across the majority of the basin. However, while weak cooling extends from surface to depth in the western Pacific, even the strong cooling in the thermocline dissipates before reaching the eastern boundary. Instead the eastern equatorial Pacific from the surface to below the thermocline features weak warming. This zonal temperature dipole is a feature of relaxed thermocline tilt: a shoaling of the western Pacific thermocline and a deepening of the eastern Pacific thermocline would respectively manifest

as a cooling and warming in depth space. The relaxed thermocline tilt in FC, caused by westerly anomalies in equatorial wind stress from a weakened Walker Circulation (not shown), agrees with Vecchi and Soden (2007)'s hypothesis that the thermocline cooling response to climate change results from a decadal Bjerknes-like response to relaxed wind stress. Additionally, slightly weakened STCs in our MF experiment (not shown) could contribute to this cooling (Yang et al., 2009; Jiang et al., 2025). We note, however, that because the MF response does not include greenhouse-gas-driven increases in subtropical stratification, and yet it accounts for all FC thermocline cooling, that this understanding disagrees with the arguments proposed by Luo et al. (2009, 2018) and Ju et al. (2022) that increased subtropical stratification creates this cooling by either slowing the STCs or advecting density-compensated anomalies.

Perhaps unsurprisingly, the BF response, which captures the ocean's response to anomalous buoyancy fluxes from increased CO_2 radiative forcing, contributes nearly all of the warming seen in FC. This includes a strong surface warming maximized in the central Pacific and most of the eastern Pacific's sub-thermocline warming. Interestingly, the central Pacific thermocline region in BF has a near-zero temperature response in the exact same region where MF cools. This allows the relatively strong momentum-driven cooling to clearly establish itself in FC. The near-zero temperature response of the BF thermocline, which strongly resembles the full centennial response to abrupt CO_2 quadrupling seen in Heede et al. (2021), also implies a relatively long-lasting upwelling damping effect.

This BF pattern, with its near-zero thermocline response, strong surface warming, and sloping sub-thermocline eastern Pacific warming, is not obviously attributable to well-known dynamics. Both conventional advective (ocean-tunnel) and dynamical (wave-driven) understandings of the STCs instead suggest broad thermocline warming. While Luongo et al. (2023) perform an ocean mixed layer heat decomposition on the equatorial SST response to NH ETINMIP forcing and attribute a certain amount of the BF SST response to ocean dynamics, the specific dynamic adjustments remain unclear. As such, we turn to MITgcm ocean-only simulations to explain the ocean dynamics that create the subsurface BF response to climate change forcing seen in Figure 2b.

3.2 Recreating the Buoyancy Response

To determine whether MITgcm is an appropriate tool with which to understand the ocean dynamics that create the buoyancy-driven mechanically-decoupled CESM1 response in Figure 2b, we first test whether MITgcm is able to effectively recreate CESM1's response at all. In the CO_2x4_BFsst OGCM simulation we add the global quasi-steady buoyancy-forced SST response to abrupt 4xCO_2 forcing (Figure 3a) to MITgcm's monthly climatological SST relaxation fields. Because we do not change any other forcing fields, the difference between this simulation and OCtrl is the ocean-only response to that SST forcing pattern.

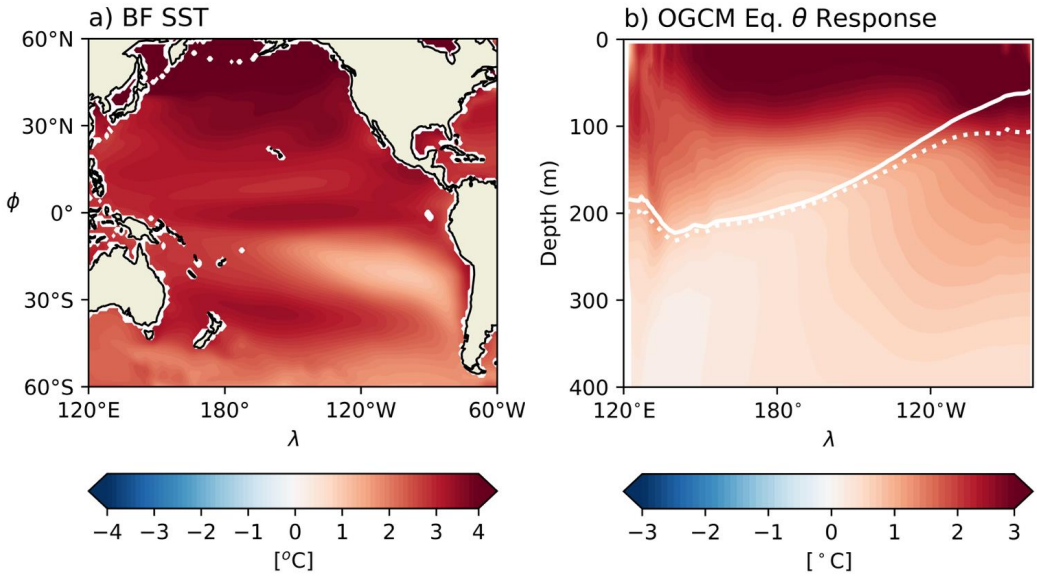

Figure 3. a) Buoyancy-forced quasi-steady (year 11-50) SST response in CESM1. b) MITgcm equatorial temperature (θ) response to BF SST forcing in panel a) averaged over years 11-30: CO_2x4_BFsst-OCtrl. The 16°C isotherm in OCtrl (solid white contour) approximates the mean thermocline and the 16°C isotherm in CO_2x4_BFsst (dotted white contour) approximates the forced thermocline.

MITgcm does a surprisingly good job of recreating the major features of CESM1's quasi-steady buoyancy-forced subsurface equatorial temperature response (c.f. Figures 2b and 3b, Pearson pattern correlation of 0.86). The MITgcm temperature response features the strong, relatively zonally symmetric near-surface warming, a warming minimum in the central-western Pacific thermocline, and sloping sub-thermocline warming

in the eastern Pacific. There are some notable differences between the two patterns, most obviously that the near-zero thermocline warming so obvious in CESM1 is deeper, more westward, and more diffuse in MITgcm. The eastern Pacific sub-thermocline warming is also weaker in MITgcm. However, MITgcm and CESM1's ocean component are different models with differences in mean state, parameterizations, and resolution. Given this reality, we consider the otherwise substantial agreement between Figures 2b and 3b to be promising, and we conclude that these ocean-only simulations are a reasonable diagnostic tool for understanding mechanically-decoupled simulations.

Having shown that the MITgcm response to the full BF SST field reasonably recreates the CESM1 response, we now ask whether we can decompose this full response further, namely into the response to SST forcing from different geographic regions. This question emerges directly from the canonical advective ocean tunnel understanding of the non-wind-driven STC response to climate change (e.g., Clement et al., 1996; Luo et al., 2009, 2017, 2018; Heede & Fedorov, 2021; Ju et al., 2022), which suggests that warm subtropical surface waters subduct in the eastern half of the subtropical gyre, are carried by mean advection to the western boundary, penetrate into the tropics via low latitude western boundary currents, and eventually warm the thermocline. Because this understanding suggests that some portion of the equatorial temperature response is entirely remotely-driven, we run two OGCM simulations to determine whether we can understand the full response to BF SST forcing as the sum of patterns created by remote and local SST forcing. We do this by regionally partitioning the full BF SST forcing field in Figure 3a into remote extratropical (ET: Figure 4a) and local equatorial (EQ: Figure 4b) SST forcing fields.

The sum of the remote (Figure 4c) and local (Figure 4d) responses almost perfectly recreates the full field response in Figure 3b (Figure S3b, Pearson pattern correlation of 0.98). However, while these patterns sum to the full response, they differ substantially and clearly represent different oceanic dynamics. We explore the ocean adjustments that create the remote and local response in the following two subsections.

3.2.1 Adjustments to Remote Buoyancy Forcing

We first consider the equatorial temperature response to extratropical-only BF SST forcing (Figure 4c). The equatorial Pacific subsurface warms in response to this remote

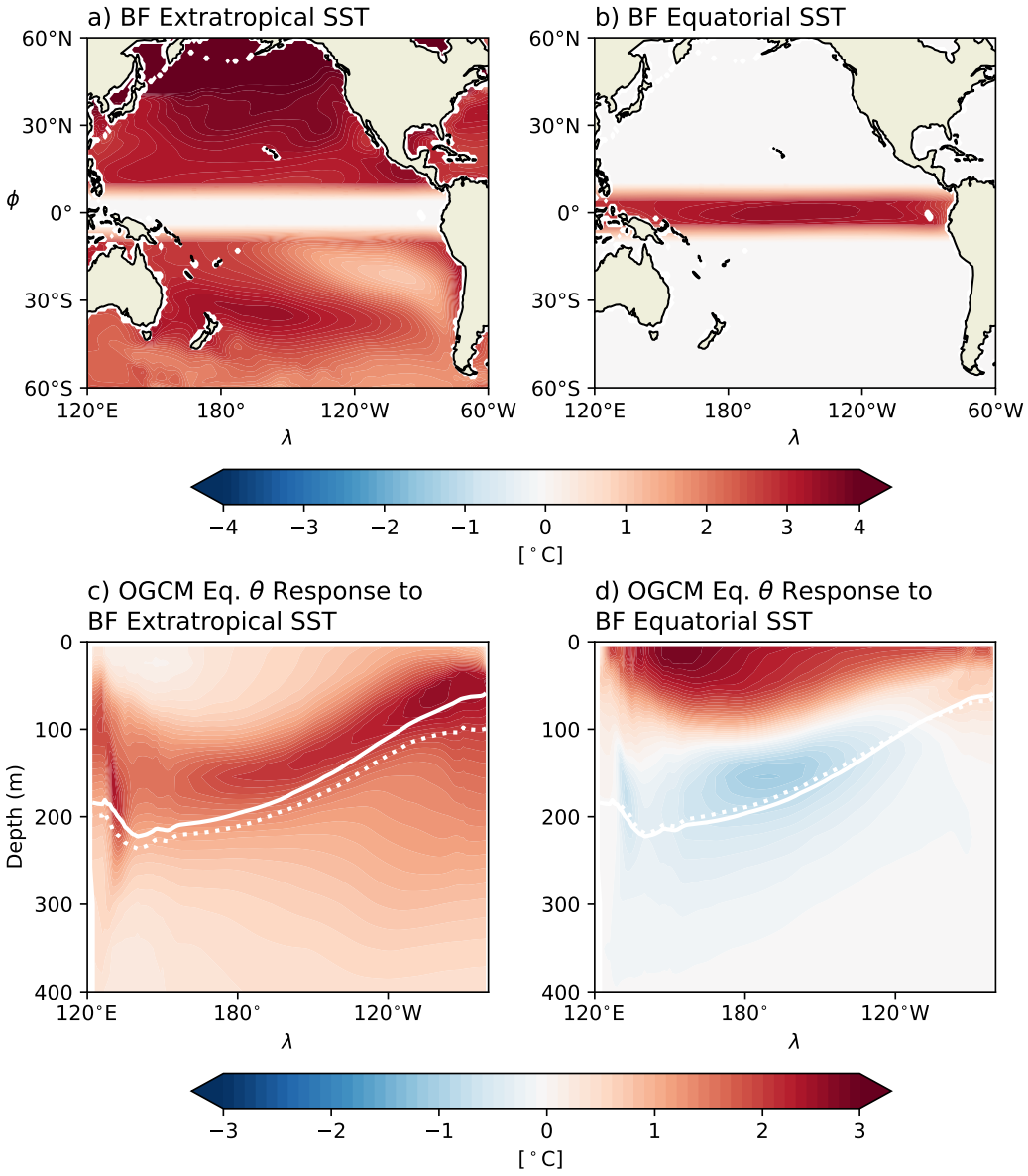

Figure 4. a) Remote, extratropical component of BF SST response in Figure 3a. b) Local, equatorial component of BF SST response in Figure 3a. c) Equatorial temperature (θ) response to remote SST forcing in panel a): CO_2x4_BFsstET-OCtrl. d) Equatorial θ response to local SST forcing in panel b): CO_2x4_BFsstEQ-OCtrl. The 16°C isotherm in OCtrl (solid white contour in panels c & d) approximates the mean thermocline and the 16°C isotherm in CO_2x4_BFsstET and CO_2x4_BFsstEQ (dotted white contours in panels c & d, respectively) approximates the perturbed thermocline.

forcing, with no evidence of cooling. The warming is maximized within the thermocline throughout the entire basin. Despite strong surface relaxation to unperturbed SSTs, the strong near-surface thermocline warming in the eastern equatorial Pacific extends to the surface. In addition, it is clear that the sloping sub-thermocline warming in the eastern Pacific noted in the FC and BF CESM1 responses above is caused by this remote adjustment.

This coherent warming of the equatorial thermocline in response to remote SST forcing in both hemispheres is strikingly similar to the equatorial temperature response to a +2°C SST anomaly in the northeast Pacific stratocumulus deck as presented in Luongo et al. (2025)'s NEPac2CWarm simulation (c.f. Figures 4c and 5b, Pearson pattern correlation of 0.94). In that study we used MITgcm to investigate how the tropical ocean responded to subtropical surface cooling. We showed that both circulation adjustments driven by baroclinic planetary waves ($\upsilon'\overline{\theta}$) and mean advection of temperature anomalies within the subtropical gyre and low latitude western boundary currents ($\overline{\upsilon}\theta'$) communicated subtropical cooling to the tropics within about a decade. At the equator, an equatorial Kelvin wave coherently heaved the thermocline as it traveled eastward. Upon hitting the eastern boundary, this wave signal radiated poleward in both hemispheres as coastal Kelvin waves, which then proceed to adjust stratification in the eastern basin by shedding westward-propagating Rossby waves. Although we primarily focused on subtropical cooling in Luongo et al. (2025), the NEPac2CWarm response presented in Figure 5 demonstrates that the equatorial temperature response to subtropical warming is simply the opposite of its response to subtropical cooling. It is also relevant to note that Luongo et al. (2025) showed that both NH and SH subtropical forcing led to similar equatorial response patterns due to the symmetric nature of the equatorial Kelvin wave adjustment.

In the case of CO_2x4_BFsstET, the dynamics clarified in Luongo et al. (2025) suggest that strong subtropical warming present in both NH and SH (Figure 4a) contribute to the warming of the equatorial thermocline (Figure 4c). This warming occurs through both mean advection of warm anomalies, as in the canonical ocean tunnel understanding, but also due to the coherent deepening of the equatorial thermocline via a downwelling Kelvin wave excited by the subtropical gyres' baroclinic response to anomalous surface warming. This dynamical adjustment is in-turn responsible for the eastern Pacific's sloping sub-thermocline warming, a slow stratification adjustment to the heaved

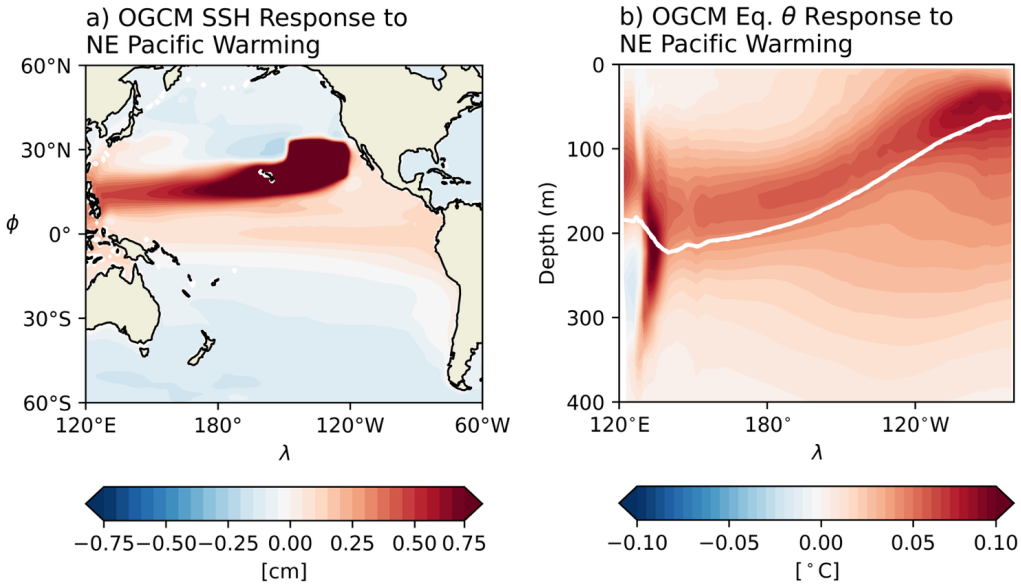

Figure 5. a) Sea surface height (SSH) response (NEPac2CWarm-OCtrl) to Northeast Pacific warming patch from Luongo et al. (2025). b) Equatorial temperature (θ) response to NEPac2CWarm simulation. The 16°C isotherm in OCtrl (solid white contour) approximates the mean thermocline and the 16°C isotherm in NEPac2CWarm (dotted white contour) approximates the forced thermocline.

thermocline. As such, while the difference in magnitude between Figures 4c and 5b results from the much stronger forcing from CO_2 quadrupling in CO_2x4_BFsstET compared to the relatively small patch of +2°C warming in NEPac2CWarm, the strong similarity in pattern re-emphasizes the importance of the STC as a dynamic mechanism to communicate subtropical warming to the equatorial thermocline.

3.2.2 Adjustments to Local Buoyancy Forcing

The response of the subsurface equatorial Pacific to the local buoyancy-forced component of climate change forcing (Figure 4d) unsurprisingly features strong near-surface warming which is directly tied to the applied tropical SST forcing (Figure 4b). However, perhaps unexpectedly, the local response features substantial cooling across much of the thermocline that underlies the strong near-surface warming. In the western Pacific, where the mean thermocline and anomalous near-surface warming signal are deepest, this thermocline cooling response extends from approximately 100-400m. As the mean thermo-

cline tilts upward to the east, this cooling signal gets shallower and thinner until the temperature anomaly switches signs to warming around 110°W. The thermocline then remains anomalously warm all the way to the eastern boundary.

Luo et al. (2018) used an OGCM to explore the response of the equatorial thermocline to a uniform tropical warming of 3.2°C. They find a pattern of near-surface warming and thermocline cooling that is similar to our response to local BF. In that work, Luo et al. (2018) suggested that this temperature response was a local baroclinic adjustment to surface warming: as near-surface stratification increases in response to surface warming, turbulent downward mixing of that heat decreases and creates a cooling signal (Yang et al., 2009). Luo et al. (2018), therefore, would attribute much of the cooling in Figure 4d to be a signal of reduced mixing. We note, however, that this mechanism does not explain the zonal temperature dipole clearly seen in our thermocline response to local BF: as discussed above, a zonal dipole instead implies a thermocline tilt and suggests the need to consider zonal gradients.

To determine whether the local response can instead be understood in terms of inviscid dynamics, we model the equatorial ocean as a simple 1.5-layer reduced gravity system. In this simplified understanding, the lower level flow is negligible compared to upper level flow ($\vec{u}_1$, $\vec{v}_1 >> \vec{u}_2$, $\vec{v}_2 = 0$), the layers are coupled by their density differences via the reduced gravity parameter [$g' \equiv g(\rho_2 - \rho_1)/\rho_2$], and the interface depth, $h = \eta + H$, is thermocline depth defined positive downward and as a sum of interface displacement η and mean thermocline depth H. Ignoring dissipation terms, the steady, linear equatorial zonal momentum equation in conservative flux form is

$$0 = -\left(g' \frac{h^2}{2}\right)_x + \frac{\tau^x}{\rho_0} \ , \tag{2}$$

where τ^x is zonal wind stress, ρ_0 is a constant reference density, and the x subscript represents a zonal derivative. If we now instead consider the non-conservative velocity form of Equation 2 linearized about H,

$$0 = -g' \eta_x + \frac{\tau^x}{\rho_0 H} \ , \tag{3}$$

and we consider a uniform Δ climate change forcing without changes in τ^x (as is the case in our OGCM simulations), the balance becomes

$$\Delta g' \overline{\eta_x} = -\overline{g'} \Delta \eta_x \ . \tag{4}$$

Equation 4 demonstrates, without making any assumptions about the eastern boundary, that the product of the perturbed RG and the mean zonal gradient of interface displacement must be balanced by the product of the mean RG and a perturbed zonal gradient of interface displacement. In the case of climate change driven warming, because $\Delta g' > 0$ we expect $\Delta \eta_x > 0$. Put another way, an increase in stratification should reduce the tilt of the thermocline even with no change in winds, in turn leading to western thermocline cooling and eastern thermocline warming.

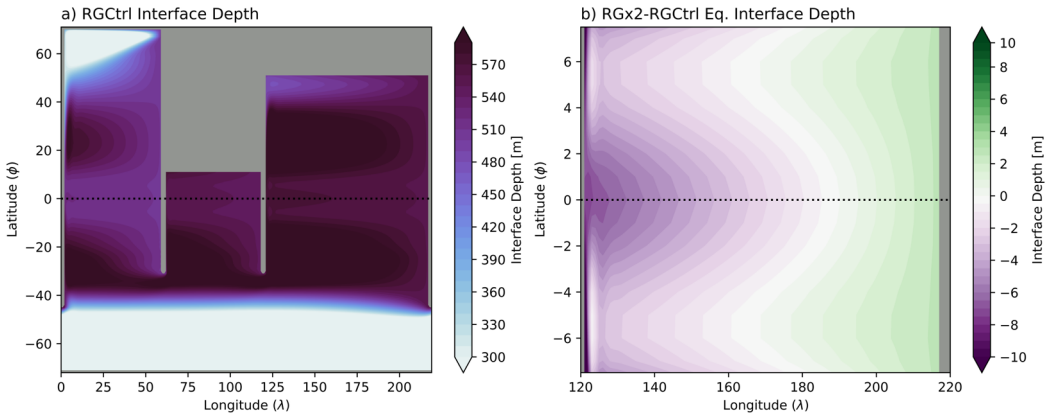

Figure 6. a) Interface depth in idealized global RG model after 20 years of spin-up in RGCtrl. b) Equatorial interface depth response to RGx2-RGCtrl's doubling of reduced gravity at year 10.

We test this tilt hypothesis with two simulations using Sun and Thompson (2020)'s idealized global ocean reduced gravity model (Figure 6a), comparing a simulation where the reduced gravity parameter is doubled (RGx2) to one where it isn't (RGCtrl). While a doubling of stratification is a relatively large forcing, it is on the same order as the near-surface equatorial Pacific increase in stratification observed in the BF response (not shown). Figure 6b shows the η response in the equatorial Pacific 10 years after RG is doubled. We see that the western equatorial Pacific interface displacement decreases (shoals), while the eastern equatorial Pacific interface displacement increases (deepens). This western Pacific shoaling and eastern Pacific deepening corresponds to a relaxation in thermocline tilt, or a western thermocline cooling and an eastern thermocline warming. We use this newly gained physical intuition to explain the thermocline temperature dipole in Fig-

ure 4d, which then adds to the coherent thermocline shoaling pointed out by Luo et al. (2018).

In summary, we conclude that the local response of the equatorial thermocline to the equatorial buoyancy-driven SST response to climate change consists of two responses to the increase in near-surface stratification: both a coherent thermocline shoaling and a decrease in thermocline tilt. This latter point questions the oft-held view that a tilted thermocline is necessarily tied to a change in zonal winds.

4 Discussion

4.1 Linearity of the Equatorial Thermocline's Response

We use a hierarchy of models to show that the full subsurface temperature response of the equatorial thermocline to greenhouse gas forcing (θ_{FC}: Figure 2a) can be recovered as a relatively simple linear combination of independent ocean dynamical responses. As in Luongo et al. (2023), we use a mechanically decoupled model to show that θ_{FC} is the sum of the wind stress-driven response (θ_{MF}: Figure 2c) and the buoyancy-driven response (θ_{BF}: Figure 2b). We then use OGCM simulations to show that θ_{BF} can be linearly partitioned into a sum of forced responses from different geographic regions of SST forcing: a remote, extratropically-driven response ($\theta_{BF,remote}$: Figure 4c) and a local, equatorially-driven response ($\theta_{BF,local}$: Figure 4d). The remote response represents the dynamically and thermodynamically-driven changes of the thermocline in response to subtropical temperature forcing, as outlined in Luongo et al. (2025). We then use a RG model to show that the local response is consistent with a response to surface stratification that includes both shoaling and reduced thermocline tilt. Putting this all together, we present this linear understanding as

$$\begin{aligned}\theta_{FC} &= \theta_{MF} + \theta_{BF} = \theta_{MF} + \theta_{BF,remote} + \theta_{BF,local} \\ &= \alpha * \mathrm{MF}(\tau^x, \tau^y) + \beta * \mathrm{BF}_{remote}(\text{NH SST, SH SST}) + \gamma * \mathrm{BF}_{local}(\text{Eq. SST}) \ . \end{aligned} \quad (5)$$

Equation 5 communicates that the full response of the modeled tropical Pacific subsurface temperature response to greenhouse gas forcing is a linear combination of ocean dynamics driven by momentum from zonal and meridional wind stress, buoyancy from NH and SH subtropical SST forcing, and buoyancy from local equatorial SST forcing,

with α, β, and γ as scaling coefficients. This is the primary result of our study. Because our FC CESM1 response to abrupt quadrupling of CO_2 strongly resembles both the 1958-2020 observed (Figure 1a) and multi-model mean (Figure 1b) response to realistic, historical climate change forcing, we conclude that this simple linear understanding gained from a hierarchy of idealized modeling simulations is a powerfully relevant and applicable tool with which to understand realistic climate change.

While this understanding is simple at face value, it in fact suggests that the equatorial temperature response to even just steady, idealized greenhouse gas forcing is more complex than previously understood. We see that the full response actually contains many of the dynamics previously suggested in the literature (e.g. Clement et al., 1996; Seager & Murtugudde, 1997; Vecchi & Soden, 2007; Luo et al., 2009, 2018; Heede et al., 2020, 2021; Watanabe et al., 2024). Nevertheless, it is only through understanding the combination of these dynamics that we can critically update our theoretical picture for how the equatorial Pacific will respond to climate change.

4.2 Reconstructing Long and Short-Term Climate Change Responses

As suggested by Equation 5, we seek to reconstruct the observed equatorial subsurface temperature trends from 1958-2020 (Figure 1a) as a linear combination of the MF and remote and local BF patterns. We use a depth-weighted ordinary least squares multilinear regression to determine combination coefficients. Our reconstruction of the 1958-2020 trend (Figure 7a) shows strong agreement with the observational composite (Figure 1a), with a Pearson pattern correlation of 0.86. We are able to explain much of both the models' and observations' long-term subsurface temperature response through our linear understanding of oceanic dynamics. Interestingly, we note that while the regression coefficients for the MF and local BF responses are positive (meaning they are in line with positive greenhouse gas forcing), the remote BF response is slightly negative (Figure 7c). This suggests that subtropical temperature forcing has not majorly impacted the equatorial thermocline in this period, and, if it has, it's been a cooling signal. This could hypothetically be due to a communication of the observed subtropical Southeast Pacific surface cooling (Wills et al., 2022) via the subtropical cells (Luongo et al., 2025).

While the multi-model mean trend is obviously similar to the observed trend over 1958-2020, the observed 1979-2020 trend is notably distinct from the modeled trend over

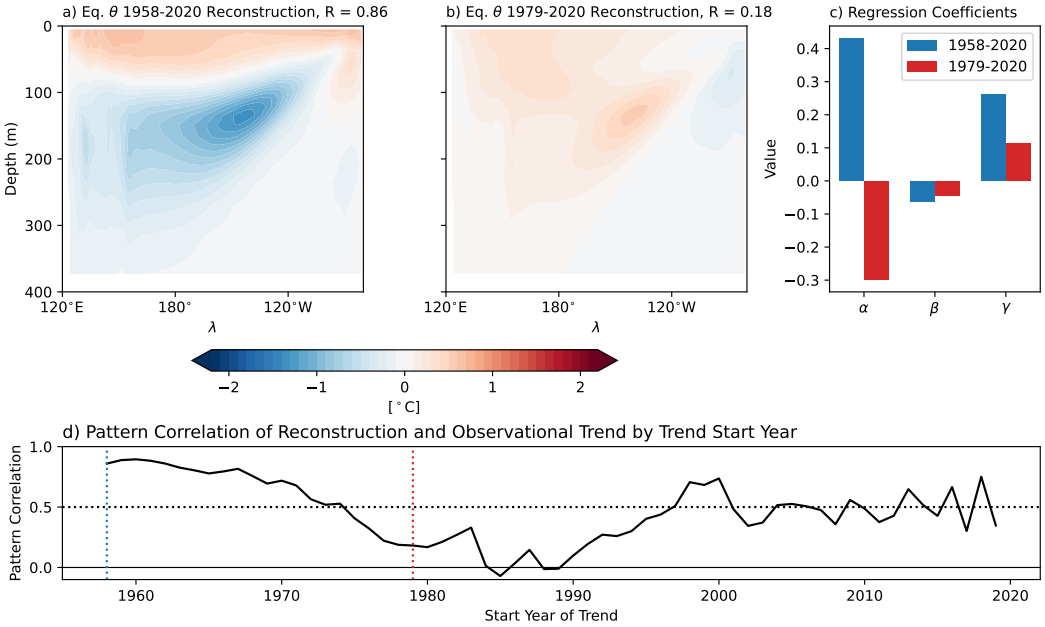

Figure 7. a) 1958-2020 reconstruction of Figure 1a observational trend using α∗MF pattern + β∗remote BF pattern + γ∗local BF pattern as in Equation 5. b) As in a), but for 1979-2020 observational trend of Figure 1c. c) Regression coefficients for linear combinations in a) and b). d) Pearson pattern correlation between regression-estimated reconstruction and observed trend as a function of trend start year. The dotted blue line highlights 1958, the dotted red line highlights 1979, and the dotted black line is at a correlation value of 0.5.

that same period (c.f. Figure 1c & d). Indeed, our multilinear regression method can not successfully reconstruct this more recent period's observed temperature trend (Figure 7b, Pearson correlation 0.18). In fact, the regression coefficients suggest that the best way to reconstruct the strong subsurface western Pacific warming in the 1979-2020 trend is via a momentum-forced response opposite to that caused by CO_2 forcing (Figure 7c). Although the understanding gained in Equation 5 works for longer-term temperature trends, it breaks down for the more recent past.

The disagreement between models' and observations' SST trends over this period has been the focus of many recent studies (e.g., Wills et al., 2022; Watanabe et al., 2024); our result underlines this disagreement further. We highlight two implications of this result. First, while Seager et al. (2019) and Jiang et al. (2025) emphasize how differences between observations and model mean states could impact SSTs, and although GCM mean states are certainly biased, the GCMs are clearly able to recreate the longer-term

subsurface temperature response to historical forcing, as long as the trend starts before ∼1975 (Figure 1e). This conclusion, combined with recent results from Dhame et al. (2025), who showed that while higher resolution simulations reduce mean state biases they do not necessarily simulate temperature trends better, suggests that mean state biases are not the only cause of disagreement in trends over the past 40 years. This suggests that despite equatorial mean state biases our climate models are not hopelessly unfit for the task of climate change projections.

Second, this result suggests an important role for internal variability in recent equatorial Pacific thermocline temperature trends: we simply cannot recreate the observed pattern of subsurface temperature since the late 1970s with our linear understanding of the ocean's response to different quasi-steady forcings. Even making the MF coefficient negative, consistent with an observed strengthening Walker circulation (L'Heureux et al., 2013), is not enough to recreate the observed dipole in the equatorial thermocline. Because our patterns are quasi-steady, internal variability is an obvious culprit. Figure 7d shows how the pattern correlation between our regression-estimated reconstruction and observational trend changes as a function of start year of the trend. Trends which start before 1975 are skillfully reconstructed from our linear understanding, presumably because enough cycles of internal variability have been averaged out to clarify the response. The linear reconstruction specifically fails, however, when attempting to reconstruct trends that begin between 1975-2000, a period when models and observations disagree the most (Figure 1e) and which also happens to coincide with several strong El Niño events.

Nevertheless, we can definitively say the dynamics we have emphasized here, decadal momentum-driven thermocline tilt, subtropical cell adjustment, and equatorial stratification-induced thermocline shoaling and tilt, contribute less to the 1979-2020 trend than has been commonly hypothesized [e.g., Figure 4 schematic of Watanabe et al. (2024)]. We hypothesize that recent internally-driven climate variability, such as ENSO or tropical Pacific decadal variability (Capotondi et al., 2023), which is not included in our pattern reconstructions, has critically crafted observed subsurface equatorial Pacific temperature trends over the past 40 years. This conclusion is in line with Jiang et al. (2024a), who emphasize the role of the Interdecadal Pacific Oscillation on SST patterns over that same period.

4.3 Implications for the Canonical Ocean Dynamical Thermostat

The simplicity of this linear understanding allows us to interrogate the canonical view of the ocean-tunnel-mediated ocean dynamical thermostat as a mechanism for understanding recent equatorial Pacific climate change. In this view, which largely rests on a mean advective understanding of the STCs ($\overline{v}\theta'$), anomalous subtropical warming is communicated to the equatorial thermocline after some lag to erode the relative cooling initially created by continued mean upwelling of unperturbed waters. As such, the conventional view of the ocean dynamical thermostat mechanism has been limited to a transient phenomenon. This understanding has been used to suggest that while the tropical Pacific's response to climate change may start as La Niña-like, as in recent observations, it will eventually transition to El Niño-like as suggested by the vast majority of model projections (Heede et al., 2020, 2021; Watanabe et al., 2024).

Our remote, buoyancy-driven response indeed shows that subtropical SST warming in the extratropics coherently warms the thermocline. While Luongo et al. (2025) show that this pattern is best understood as having been created by wave dynamics, the basic understanding that subtropical SSTs warm the equatorial thermocline via the STCs holds true. In the framework of the upwelling damping effect of mean vertical advection on equatorial SSTs (-$\overline{w}\theta'_z \equiv -\overline{w}\frac{\theta'_s-\theta'_e}{H_e}$: e.g., Xie et al., 2010), where the s and e subscripts are respectively surface and entrainment levels and H_e is the depth of the entrainment level to the surface, initially $\theta'_e < \theta'_s$ and so mean upwelling cools, but eventually $\theta'_e > \theta'_s$ and mean upwelling warms.

However, our remote and local MITgcm simulations show that this is a delicate balance: the remotely-driven thermocline warming (Figure 4c) is entirely canceled out (Figure 2b & 3b) by the locally-driven thermocline cooling (Figure 4d). In the case of our simulations, subtropical warming only works to erode the local cooling from thermocline shoaling and decreased thermocline tilt such that the final, steady thermocline temperature response is near-zero ($\theta'_e \approx 0$) and there is no sign change in $-\overline{w}\theta'_z$ with time. This implies a long-lasting upwelling damping effect. Our model simulations, therefore, suggest that the canonical view of the thermostat necessarily leading to a transient response (as has been used to explain recent observations) is misleading. Rather, we emphasize that the relative ratio of tropically-driven cooling to extratropically-driven warming is critical to understand timescales associated with the buoyancy-driven response. In our

case, which in turn resembles the near-steady, centennial response to abrupt quadrupling of CO_2 (Heede et al., 2021), remote warming simply cancels out local cooling such that there is no major warming of the thermocline from SST forcing at all (Figures 2b & 3b). If instead, however, the extratropically-driven warming was much larger than the tropically-driven cooling we might expect a correlation between subtropical to tropical meridional SST gradients and the tropical zonal SST gradient (Burls & Fedorov, 2014). Considered together, we instead hypothesize that the more likely driver of transience in the surface response results from a change in the momentum-driven pattern or other atmospheric pathways.

4.4 Symmetry of Equatorial Responses

A final surprising detail of this study is the immutability of the equatorial Pacific subsurface temperature response regardless of forcing geography. This is best seen by comparing the FC, BF, and MF responses to abrupt quadrupling of CO_2 (Figure 2) to those same responses to NH and SH ETINMIP forcing (Figure S4). Despite the fact that CO_2 forcing is primarily equatorially symmetric and ETINMIP forcing is purposefully equatorially asymmetric, the response patterns are effectively the same (with an opposite sign). From the perspective of the equatorial Pacific subsurface, it would be difficult to immediately tell the difference between greenhouse gas warming and a hypothetical extratropical warming (e.g., Tseng et al., 2023). This similarity extends to the linear partitioning of the buoyancy-driven response into remote and local forcing (Figure S5). The equatorially symmetric nature of the equatorial thermocline's response to subtropical forcing (Luongo et al., 2025) creates the same remote response pattern as if both hemispheres' subtropics were forced. Because the local response just depends on an increase or decrease in surface stratification, the equatorial response to local forcing looks effectively the same.

This understanding raises two interesting points. First, it highlights that hemispheric asymmetries in meridional forcing, crucial to the zonal-mean energetic framework through which we understand ITCZ shifts (Kang et al., 2008) and cross-equatorial ocean heat transport (Luongo et al., 2022), do not lead to appreciably different equatorial temperature responses. Despite the fact that ETINMIP forcing drives strong cross-equatorial responses, the equatorial thermocline simply cares if the forcing causes large-scale warming or cooling. Second, the equatorial thermocline's response to industrial aerosol forc-

ing (similar to NH ETINMIP forcing) would not lead to an independent temperature pattern from greenhouse gas forcing. Put another way, NH aerosol forcing would simply modulate the tropical Pacific's response to greenhouse gas forcing rather than create a fundamentally different pattern.

5 Conclusions

In this study we have used a series of climate modeling simulations of varied complexity to understand the equatorial thermocline response to climate change. We first show that a multi-model mean of 11 large ensembles reasonably captures the observed 1958-2020 subsurface equatorial temperature trend, and that CESM1's 11-50 year average response to abrupt quadrupling of CO_2 is an appropriate tool with which to understand the models' response to realistic, historical forcing. We then decompose the full equatorial thermocline response into a response due to buoyancy forcing alone and momentum forcing alone, the latter of which drives thermocline cooling. We use an ocean-only GCM with anomalous SST forcing to further decompose that buoyancy-forced component, and we demonstrate that the response due to extratropical SST forcing and tropical SST forcing linearly combine to recreate the full field buoyancy-forced response. The remote, extratropically-driven response leads to a coherent thermocline warming through dynamic and thermodynamic pathways. The increase in near-surface stratification in the local, tropically-driven response leads to both a shoaling thermocline and a relaxation of thermocline tilt. Our primary finding is that a simple linear combination of these adjustments, i) momentum-driven, ii) remote buoyancy-driven, and iii) local buoyancy-driven, skillfully explains both the long-term 1958-2020 modeled and observed responses. We can attribute certain features of the pattern to certain dynamics: we agree with Vecchi and Soden (2007) and Jiang et al. (2025)'s suggestion that the thermocline cooling response to global warming results from momentum-driven dynamics. However, this dynamical understanding does not explain more recent trends (e.g., the 1979-2020 response), suggesting that this period was strongly affected by internal variability.

Our results emphasize that the subsurface equatorial Pacific temperature response to climate change is a highly linear system. This linearity is powerful. It allows us to test long-held theoretical understandings, such as how subtropical warming will affect the transient adjustment of the tropical thermocline or that changes in zonal wind stress are necessary for a thermocline tilt. While this study does not answer what has caused recent

subsurface mismatches between models and observations or whether models are missing a hypothetical forcing that might explain that mismatch, we demonstrate that model mean states are not so irreparably biased that we cannot learn from them. Instead, these models clarify the specific patterns created by commonly referenced ocean dynamic adjustments. In a practical sense, we also outline a clear model hierarchy, fully-coupled, mechanically-decoupled, ocean-only, and reduced gravity, which could be potentially leveraged to comprehend other coupled climate responses.

6 Open Research

The climate model output used in this study will be made freely available on Zenodo upon study publication. A draft repository for peer review is available at the link in the supporting documentation.

7 Conflict of Interest Statement

The authors have no conflicts of interest to disclose.

Acknowledgments

MTL was supported by the Cooperative Institute for Climate, Ocean, & Ecosystem Studies (CICOES) under NOAA Cooperative Agreement NA20OAR4320271, Contribution No. 2026-1538. IE was supported by National Science Foundation (NSF) award OCE-2048590. KCA was supported by NSF award AGS-2203543 and a Calvin Professorship in Oceanography. We thank UCAR and NSF for providing exploratory allocations of core hours on the Cheyenne and Derecho supercomputers. We sincerely thank Feng Jiang for providing the ensemble mean model data used in Figure 1b & d, and without implying endorsement, we thank Natalie Burls for helpful discussion. We also thank our editor, Dr. Xin Wang, and three anonymous reviewers for thoughtful and constructive feedback that greatly improved this study.

References

Baldwin, J. W., Atwood, A. R., Vecchi, G. A., & Battisti, D. S. (2021). Outsize Influence of Central American Orography on Global Climate. *AGU Advances*, *2*(2), e2020AV000343.

Bjerknes, J. (1969). Atmospheric Teleconnections from the Equatorial Pacific. *Monthly weather review*, *97*(3), 163–172.

Burls, N., & Fedorov, A. (2014). What Controls the Mean East–West Sea Surface Temperature Gradient in the Equatorial Pacific: The Role of Cloud Albedo. *Journal of Climate*, *27*(7), 2757–2778.

Capotondi, A., McGregor, S., McPhaden, M. J., Cravatte, S., Holbrook, N. J., Imada, Y., ... others (2023). Mechanisms of Tropical Pacific Decadal Variability. *Nature Reviews Earth & Environment*, *4*(11), 754–769.

Carton, J. A., & Giese, B. S. (2008). A Reanalysis of Ocean Climate Using Simple Ocean Data Assimilation (SODA). *Monthly weather review*, *136*(8), 2999–3017.

Clement, A. C., Seager, R., Cane, M. A., & Zebiak, S. E. (1996). An Ocean Dynamical Thermostat. *Journal of Climate*, *9*(9), 2190–2196.

Coats, S., & Karnauskas, K. (2017). Are Simulated and Observed Twentieth Century Tropical Pacific Sea Surface Temperature Trends Significant Relative to Internal Variability? *Geophysical Research Letters*, *44*(19), 9928–9937.

Dhame, S., Olonscheck, D., & Rugenstein, M. (2025). Higher-Resolution Climate Models Do Not Consistently Reproduce the Observed Tropical Pacific Warming Pattern. *Journal of Climate*, *38*(13), 3131–3149.

DiNezio, P. N., Clement, A. C., Vecchi, G. A., Soden, B. J., Kirtman, B. P., & Lee, S.-K. (2009). Climate Response of the Equatorial Pacific to Global Warming. *Journal of Climate*, *22*(18), 4873–4892.

Dong, Y., Armour, K. C., Battisti, D. S., & Blanchard-Wrigglesworth, E. (2022). Two-way Teleconnections between the Southern Ocean and the Tropical Pacific via a Dynamic Feedback. *Journal of Climate*, *35*(19), 6267–6282.

Forget, G., Campin, J.-M., Heimbach, P., Hill, C., Ponte, R., & Wunsch, C. (2015). ECCO Version 4: An Integrated Framework for Non-Linear Inverse Modeling and Global Ocean State Estimation. *Geoscientific Model Development*, *8*(10), 3071–3104.

Good, S. A., Martin, M. J., & Rayner, N. A. (2013). EN4: Quality Controlled Ocean Temperature and Salinity Profiles and Monthly Objective Analyses with Uncertainty Estimates. *Journal of Geophysical Research: Oceans*, *118*(12), 6704–6716.

Heede, U. K., & Fedorov, A. V. (2021). Eastern Equatorial Pacific Warming Delayed by Aerosols and Thermostat Response to

$CO_2 Increase. Nature\ Climate\ Change, 11(8), 696 - -703.$

Heede, U. K., & Fedorov, A. V. (2023). Colder Eastern Equatorial Pacific and Stronger Walker Circulation in the Early 21st Century: Separating the Forced Response to Global Warming from Natural Variability. *Geophysical Research Letters*, *50*(3), e2022GL101020.

Heede, U. K., Fedorov, A. V., & Burls, N. J. (2020). Time Scales and Mechanisms for the Tropical Pacific Response to Global Warming: A Tug of War between the Ocean Thermostat and Weaker Walker. *Journal of Climate*, *33*(14), 6101–6118.

Heede, U. K., Fedorov, A. V., & Burls, N. J. (2021). A Stronger versus Weaker Walker: Understanding Model Differences in Fast and Slow Tropical Pacific Responses to Global Warming. *Climate Dynamics*, *57*(9), 2505–2522.

Horel, J. D., & Wallace, J. M. (1981). Planetary-scale Atmospheric Phenomena Associated with the Southern Oscillation. *Monthly Weather Review*, *109*(4), 813–829.

Hurrell, J. W., Holland, M. M., Gent, P. R., Ghan, S., Kay, J. E., Kushner, P. J., ... others (2013). The Community Earth System Model: A Framework for Collaborative Research. *Bulletin of the American Meteorological Society*, *94*(9), 1339–1360.

Hwang, Y.-T., Xie, S.-P., Chen, P.-J., Tseng, H.-Y., & Deser, C. (2024). Contribution of Anthropogenic Aerosols to Persistent La Niña-like Conditions in the Early 21st Century. *Proceedings of the National Academy of Sciences*, *121*(5), e2315124121.

Ishii, M., & Kimoto, M. (2009). Reevaluation of Historical Ocean Heat Content Variations with Time-Varying XBT and MBT Depth Bias Corrections. *Journal of Oceanography*, *65*(3), 287–299.

Jiang, F., Seager, R., & Cane, M. A. (2024a). A Climate Change Signal in the Tropical Pacific Emerges from Decadal Variability. *Nature Communications*, *15*(1), 8291.

Jiang, F., Seager, R., & Cane, M. A. (2024b). Historical Subsurface Cooling in the Tropical Pacific and its Dynamics. *Journal of Climate*, *37*(22), 5925–5938.

Jiang, F., Seager, R., Cane, M. A., Karamperidou, C., & Brizuela, N. G. (2025). Subsurface Cooling and Sea Surface Temperature Pattern Formation over

805 the Equatorial Pacific. *Journal of Geophysical Research: Oceans*, *130*(4),
806 e2024JC022222.

807 Ju, W.-S., Zhang, Y., & Du, Y. (2022). Subsurface Cooling in the Tropical Pacific
808 under a Warming Climate. *Journal of Geophysical Research: Oceans*, *127*(5),
809 e2021JC018225.

810 Kang, S. M., Hawcroft, M., Xiang, B., Hwang, Y.-T., Cazes, G., Codron, F., ...
811 others (2019). Extratropical–Tropical Interaction Model Intercomparison
812 Project (ETIN-MIP): Protocol and Initial Results. *Bulletin of the American*
813 *Meteorological Society*, *100*(12), 2589–2606.

814 Kang, S. M., Held, I. M., Frierson, D. M., & Zhao, M. (2008). The Response of the
815 ITCZ to Extratropical Thermal Forcing: Idealized Slab-Ocean Experiments
816 with a GCM. *Journal of Climate*, *21*(14), 3521–3532.

817 Kang, S. M., Shin, Y., Kim, H., Xie, S.-P., & Hu, S. (2023). Disentangling the
818 Mechanisms of Equatorial Pacific Climate Change. *Science Advances*, *9*(19),
819 eadf5059.

820 Karnauskas, K. B., Seager, R., Kaplan, A., Kushnir, Y., & Cane, M. A. (2009).
821 Observed Strengthening of the Zonal Sea Surface Temperature Gradient across
822 the Equatorial Pacific Ocean. *Journal of Climate*, *22*(16), 4316–4321.

Knutson, T. R., & Manabe, S. (1995). Time-mean Response over the Tropical Pacific to Increased $CO_2 in a Coupled Ocean - Atmosphere Model$. *Journal of Climate*, *8*(9), 2181 – −2199.

823 Kosaka, Y., & Xie, S.-P. (2016). The Tropical Pacific as a Key Pacemaker of the
824 Variable Rates of Global Warming. *Nature Geoscience*, *9*(9), 669–673.

825 Laepple, T., & Huybers, P. (2014). Ocean Surface Temperature Variability: Large
826 Model-Data Differences at Decadal and Longer Periods. *Proceedings of the Na-*
827 *tional Academy of Sciences*, *111*(47), 16682–16687.

828 Liu, Z. (1994). A Simple Model of the Mass Exchange between the Subtropical and
829 Tropical Ocean. *Journal of Physical Oceanography*, *24*(6), 1153–1165.

830 Luo, Y., Liu, F., & Lu, J. (2018). Response of the Equatorial Pacific Thermocline to
831 Climate Warming. *Ocean Dynamics*, *68*(11), 1419–1429.

832 Luo, Y., Lu, J., Liu, F., & Garuba, O. (2017). The Role of Ocean Dynamical Ther-
833 mostat in Delaying the El Niño–like Response over the Equatorial Pacific to
834 Climate Warming. *Journal of Climate*, *30*(8), 2811–2827.

Luo, Y., Rothstein, L. M., & Zhang, R.-H. (2009). Response of Pacific Subtropical-Tropical Thermocline Water Pathways and Transports to Global Warming. *Geophysical Research Letters*, *36*(4).

Luongo, M. T., Brizuela, N. G., Eisenman, I., & Xie, S.-P. (2024). Retaining Short-term Variability Reduces Mean State Biases in Wind Stress Overriding Simulations. *Journal of Advances in Modeling Earth Systems*, *16*(2), e2023MS003665.

Luongo, M. T., Xie, S.-P., & Eisenman, I. (2022). Buoyancy forcing dominates the cross-equatorial ocean heat transport response to Northern Hemisphere extratropical cooling. *Journal of Climate*, *35*(20), 6671–6690.

Luongo, M. T., Xie, S.-P., Eisenman, I., Hwang, Y.-T., & Tseng, H.-Y. (2023). A Pathway for Northern Hemisphere Extratropical Cooling to Elicit a Tropical Response. *Geophysical Research Letters*, *50*(2), e2022GL100719.

Luongo, M. T., Xie, S.-P., Eisenman, I., Sun, S., & Peng, Q. (2025). How the Subsurface Tropical Pacific Responds to Subtropical Surface Cooling: Implications for Cross-Equatorial Transport. *Journal of Climate*.

L'Heureux, M. L., Lee, S., & Lyon, B. (2013). Recent Multidecadal Strengthening of the Walker Circulation across the Tropical Pacific. *Nature Climate Change*, *3*(6), 571–576.

Mantua, N. J., Hare, S. R., Zhang, Y., Wallace, J. M., & Francis, R. C. (1997). A Pacific Interdecadal Climate Oscillation with Impacts on Salmon Production. *Bulletin of the american Meteorological Society*, *78*(6), 1069–1080.

McCreary Jr, J. P., & Lu, P. (1994). Interaction between the Subtropical and Equatorial Ocean Circulations: The Subtropical Cell. *Journal of Physical Oceanography*, *24*(2), 466–497.

McGregor, S., Stuecker, M. F., Kajtar, J. B., England, M. H., & Collins, M. (2018). Model Tropical Atlantic Biases Underpin Diminished Pacific Decadal Variability. *Nature Climate Change*, *8*(6), 493–498.

Merlis, T. M., & Schneider, T. (2011). Changes in Zonal Surface Temperature Gradients and Walker Circulations in a Wide Range of Climates. *Journal of climate*, *24*(17), 4757–4768.

Olonscheck, D., Rugenstein, M., & Marotzke, J. (2020). Broad Consistency between Observed and Simulated Trends in Sea Surface Temperature Patterns.

Geophysical Research Letters, *47*(10), e2019GL086773.

Peng, Q., Xie, S.-P., Wang, D., Huang, R. X., Chen, G., Shu, Y., ... Liu, W. (2022). Surface Warming–Induced Global Acceleration of Upper Ocean Currents. *Science Advances*, *8*(16), eabj8394.

Philander, S. G. H. (1983). El Niño Southern Oscillation Phenomena. *Nature*, *302*(5906), 295–301.

Seager, R., Cane, M., Henderson, N., Lee, D.-E., Abernathey, R., & Zhang, H. (2019). Strengthening Tropical Pacific Zonal Sea Surface Temperature Gradient Consistent with Rising Greenhouse Gases. *Nature Climate Change*, *9*(7), 517–522.

Seager, R., Henderson, N., & Cane, M. (2022). Persistent Discrepancies between Observed and Modeled Trends in the Tropical Pacific Ocean. *Journal of Climate*, *35*(14), 4571–4584.

Seager, R., & Murtugudde, R. (1997). Ocean Dynamics, Thermocline Adjustment, and Regulation of Tropical SST. *Journal of climate*, *10*(3), 521–534.

Solomon, A., & Newman, M. (2012). Reconciling Disparate Twentieth-century Indo-Pacific Ocean Temperature Trends in the Instrumental Record. *Nature Climate Change*, *2*(9), 691–699.

Sun, S., & Thompson, A. F. (2020). Centennial Changes in the Indonesian Throughflow Connected to the Atlantic Meridional Overturning Circulation: The Ocean's Transient Conveyor Belt. *Geophysical Research Letters*, *47*(21), e2020GL090615.

Taylor, B. A., Shi, J.-R., Xie, S.-P., Talley, L. D., Luongo, M. T., & Peng, Q. (2025). Warming Band in Southern Ocean's Indian Sector: The Role of Remote Atlantic Buoyancy Forcing via Poleward-Shifting Circulation Response. *Journal of Climate*, *38*(14), 3219–3238.

Tseng, H.-Y., Hwang, Y.-T., Xie, S.-P., Tseng, Y.-H., Kang, S. M., Luongo, M. T., & Eisenman, I. (2023). Fast and Slow Responses of the Tropical Pacific to Radiative Forcing in Northern High Latitudes. *Journal of Climate*, *36*(16), 5337–5349.

Tuchen, F. P., Perez, R. C., Foltz, G. R., McPhaden, M. J., & Lumpkin, R. (2024). Strengthening of the Equatorial Pacific Upper-Ocean Circulation over the Past Three Decades. *Journal of Geophysical Research: Oceans*, *129*(11),

e2024JC021343.

Vecchi, G. A., & Soden, B. J. (2007). Global Warming and the Weakening of the Tropical Circulation. *Journal of Climate*, *20*(17), 4316–4340.

Watanabe, M., Dufresne, J.-L., Kosaka, Y., Mauritsen, T., & Tatebe, H. (2021). Enhanced Warming Constrained by Past Trends in Equatorial Pacific Sea Surface Temperature Gradient. *Nature Climate Change*, *11*(1), 33–37.

Watanabe, M., Kang, S. M., Collins, M., Hwang, Y.-T., McGregor, S., & Stuecker, M. F. (2024). Possible Shift in Controls of the Tropical Pacific Surface Warming Pattern. *Nature*, *630*(8016), 315–324.

Wills, R. C., Dong, Y., Proistosecu, C., Armour, K. C., & Battisti, D. S. (2022). Systematic Climate Model Biases in the Large-scale Patterns of Recent Sea-surface Temperature and Sea-level Pressure Change. *Geophysical Research Letters*, *49*(17), e2022GL100011.

Wyrtki, K. (1975). El Niño—The Dynamic Response of the Equatorial Pacific Ocean to Atmospheric Forcing. *Journal of Physical Oceanography*, *5*(4), 572–584.

Xie, S.-P., Deser, C., Vecchi, G. A., Ma, J., Teng, H., & Wittenberg, A. T. (2010). Global Warming Pattern Formation: Sea Surface Temperature and Rainfall. *Journal of Climate*, *23*(4), 966–986.

Yang, H., Wang, F., & Sun, A. (2009). Understanding the ocean temperature change in global warming: the tropical Pacific. *Tellus A: Dynamic Meteorology and Oceanography*, *61*(3), 371–380.

Zuo, H., Balmaseda, M. A., Tietsche, S., Mogensen, K., & Mayer, M. (2019). The ECMWF Operational Ensemble Reanalysis–Analysis System for Ocean and Sea Ice: A Description of the System and Assessment. *Ocean science*, *15*(3), 779–808.

Supporting Information for "Explaining the Equatorial Pacific Thermocline Response to Climate Change with a Model Hierarchy"

Matthew T. Luongo[1,2], Shang-Ping Xie[3], Ian Eisenman[3], Shantong Sun[4], &

Kyle C. Armour[2,5]

[1]Cooperative Institute for Climate, Ocean, & Ecosystem Studies, University of Washington, Seattle, WA

[2]School of Oceanography, University of Washington, Seattle, WA

[3]Scripps Institution of Oceanography, UC San Diego, La Jolla, CA

[4]Laoshan Laboratory, Qingdao, China

[5]Department of Atmospheric & Climate Science, University of Washington, Seattle, WA

Contents of this file Table S1 and Figures S1-S5.

References

Carton, J. A., & Giese, B. S. (2008). A Reanalysis of Ocean Climate Using Simple Ocean Data Assimilation (SODA). *Monthly weather review*, *136*(8), 2999–3017.

Good, S. A., Martin, M. J., & Rayner, N. A. (2013). EN4: Quality Controlled Ocean Temperature and Salinity Profiles and Monthly Objective Analyses with Uncertainty Estimates. *Journal of Geophysical Research: Oceans*, *118*(12), 6704–6716.

Ishii, M., & Kimoto, M. (2009). Reevaluation of Historical Ocean Heat Content Variations with Time-Varying XBT and MBT Depth Bias Corrections. *Journal of Oceanography*, *65*(3), 287–299.

Jiang, F., Seager, R., Cane, M. A., Karamperidou, C., & Brizuela, N. G. (2025). Subsurface Cooling and Sea Surface Temperature Pattern Formation over the Equatorial Pacific. *Journal of Geophysical Research: Oceans*, *130*(4), e2024JC022222.

Kang, S. M., Hawcroft, M., Xiang, B., Hwang, Y.-T., Cazes, G., Codron, F., ... others (2019). Extratropical–Tropical Interaction Model Intercomparison Project (ETIN-MIP): Protocol and Initial Results. *Bulletin of the American Meteorological Society*, *100*(12), 2589–2606.

Zuo, H., Balmaseda, M. A., Tietsche, S., Mogensen, K., & Mayer, M. (2019). The ECMWF Operational Ensemble Reanalysis–Analysis System for Ocean and Sea Ice: A Description of the System and Assessment. *Ocean science*, *15*(3), 779–808.

Fully-coupled Simulations			
Simulation Name	**CO_2 Forcing**	**Wind Stress**	**ETINMIP Forcing**
ETINMIPNH	280ppm	Freely evolving	45°N–65°N
ETINMIPSH	280ppm	Freely evolving	45°S–65°S
Mechanically-decoupled Simulations			
Simulation Name	**CO_2 Forcing**	**Wind Stress**	**ETINMIP Forcing**
Tau_1_S_NH	280ppm	Ctrl	45°N–65°N
Tau_NH_S_1	280ppm	ETINMIPNH	n/a
Tau_1_S_SH	280ppm	Ctrl	45°S–65°S
Tau_SH_S_1	280ppm	ETINMIPSH	n/a
Ocean-only Simulations			
Simulation Name	**SST Forcing Perturbation**	**SST Forcing Bounds**	
ETINMIPNH_BFsst	Tau_1_S_NH-Tau1CO_2x1	90°S-90°N	
ETINMIPNH_BFsstET	Tau_1_S_NH-Tau1CO_2x1	90°S-6°S, 6°N-90°N	
ETINMIPNH_BFsstEQ	Tau_1_S_NH-Tau1CO_2x1	10°S-10°N	
ETINMIPSH_BFsst	Tau_1_S_SH-Tau1CO_2x1	90°S-90°N	
ETINMIPSH_BFsstET	Tau_1_S_SH-Tau1CO_2x1	90°S-6°S, 6°N-90°N	
ETINMIPSH_BFsstEQ	Tau_1_S_SH-Tau1CO_2x1	10°S-10°N	

Table S1. Details of fully coupled, mechanically-decoupled, and ocean-only simulations using top-of-atmosphere hemispherically asymmetric extratropical forcing from the Extratropical-Tropical Interaction Model Intercomparison Project (ETINMIP: Kang et al., 2019). The Ctrl and Tau1CO_2x1 simulations are described in Table 1 of the main text.

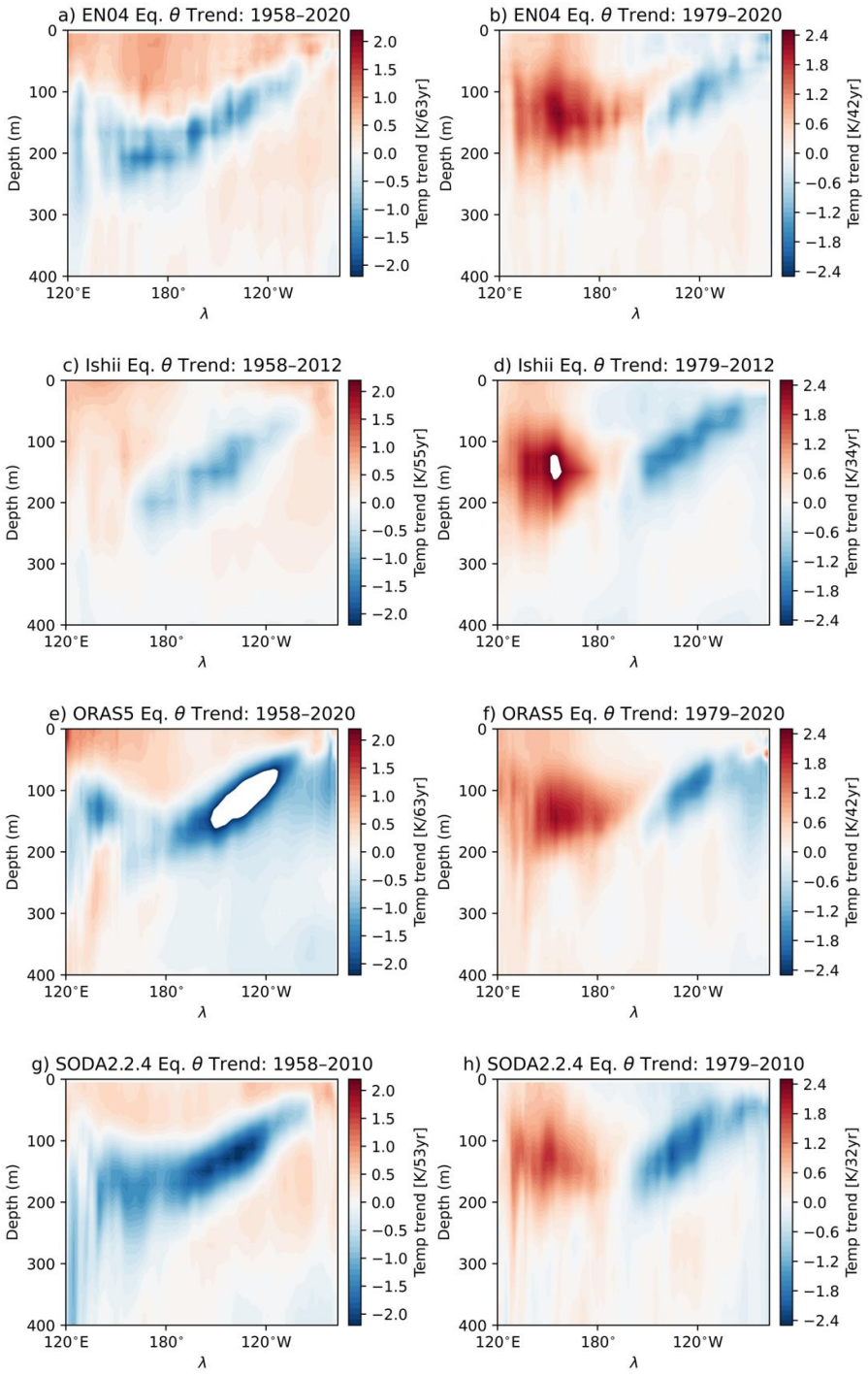

Figure S1. Equatorial subsurface temperature (θ) trend for EN04 observational product (top row, Good et al., 2013), Ishii observational product (second row, Ishii & Kimoto, 2009), ORAS5 ocean reanalysis (third row, Zuo et al., 2019), and SODA2.2.4 ocean reanalysis (fourth row, Carton & Giese, 2008) While time periods depend on specific data source, longer-term trends are in the left column and shorter-term trends in the right column.

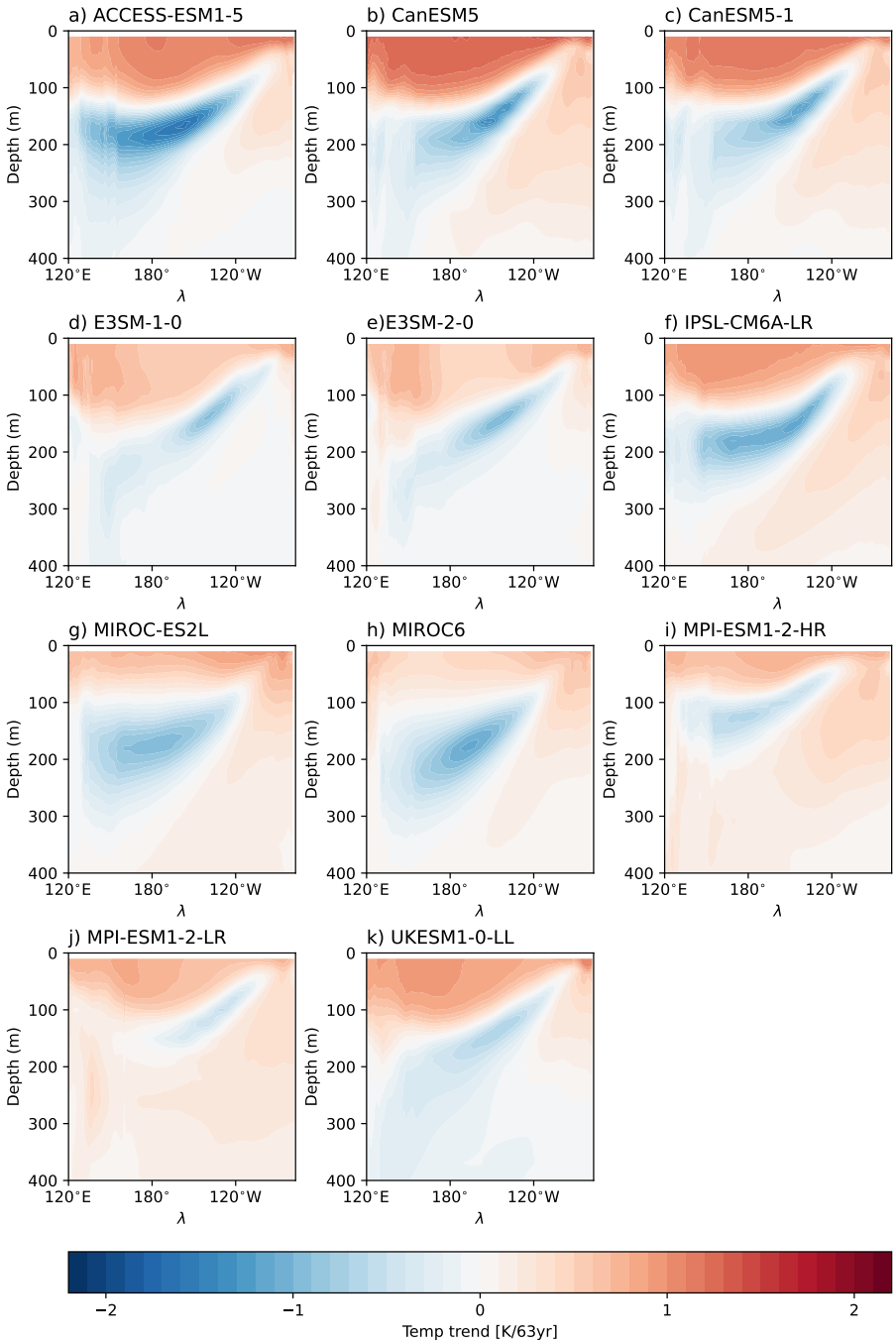

Figure S2. Ensemble mean 1958-2020 equatorial subsurface temperature (θ) trend for a) ACCESS-ESM1-5, b) CanESM5, c) CanESM5-1, d) E3SM-1-0, e) E3SM-2-0, f) IPSL-CM6A-LR, g) MIROC-ES2L, h) MIROC6, i) MPI-ESM1-2-HR, j) MPI-ESM1-2-LR, and k) UKESM1-0-LL large ensembles as selected by Jiang et al. (2025). Ensembles are forced by historical forcing from 1958-2014 and from 2015-2020 by the Shared Socioeconomic Pathway 3-7.5 scenario.

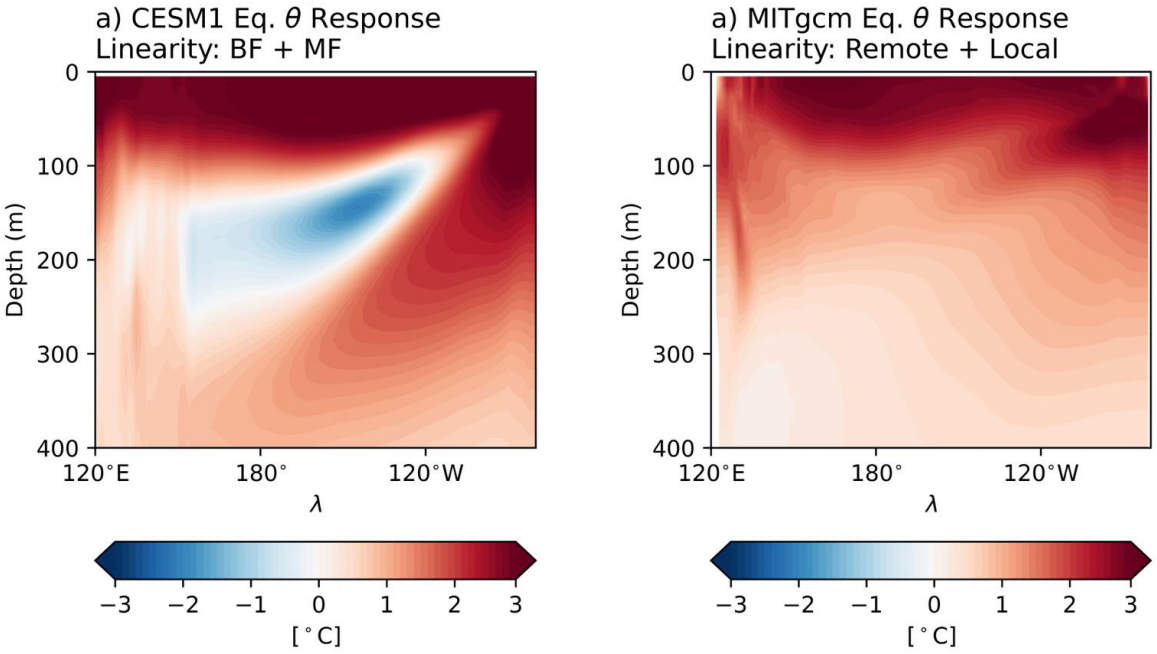

Figure S3. a) Linearity of CESM1 equatorial temperature (θ) response to abrupt quadrupling of CO_2: Sum of buoyancy-forced (BF = Tau1CO_2x4-Tau1CO_2x1, Figure 2b of the main text) response and momentum-forced (MF = Tau4CO_2x1-Tau1CO_2x1, Figure 2c of the main text) response. Compare this sum with the FC response (Figure 2a of the main text). b) Linearity of the MITgcm equatorial θ response to BF SST forcing: Sum of response to remote SST forcing (CO_2x4_BFsstET-OCtrl, Figure 4c of the main text) and response to local SST forcing (CO_2x4_BFsstEQ-OCtrl, Figure 4d of the main text). Compare this sum with the full field response (Figure 3b of the main text).

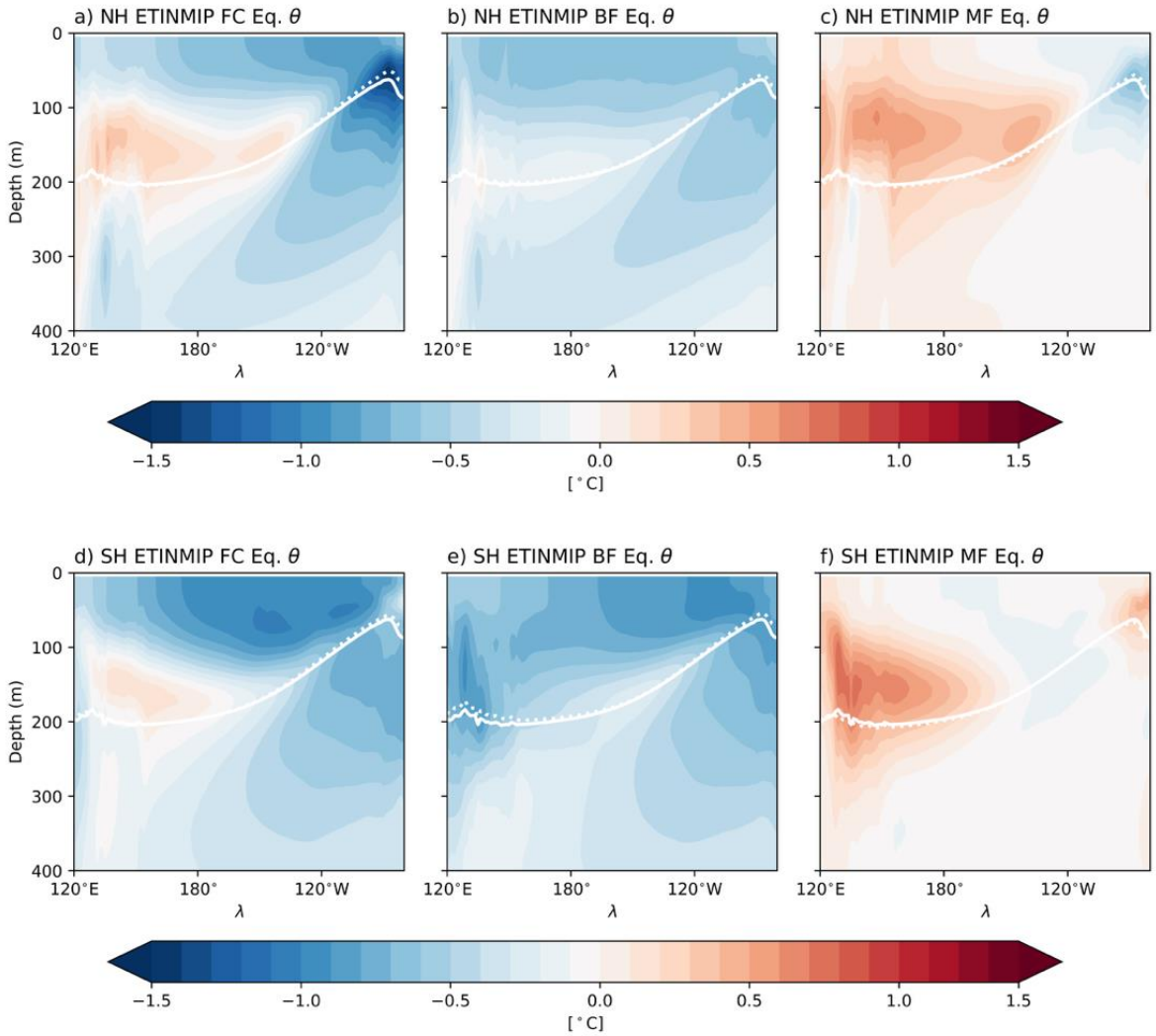

Figure S4. a) CESM1 fully-coupled (FC = ETINMIPNH-Ctrl) equatorial temperature (θ) response to Northern Hemisphere (NH) ETINMIP forcing. b) CESM1 buoyancy-forced (BF = Tau_1_S_NH-Tau1CO_2x1) equatorial θ response to NH ETINMIP forcing. c) CESM1 momentum-forced (MF = Tau_NH_S_1-Tau1CO_2x1) equatorial θ response to NH ETINMIP forcing. d) CESM1 FC (ETINMIPSH-Ctrl) equatorial θ response to Southern Hemisphere (SH) ETINMIP forcing. e) CESM1 BF (Tau_1_S_SH-Tau1CO_2x1) equatorial θ response to SH ETINMIP forcing. f) CESM1 MF (Tau_SH_S_1-Tau1CO_2x1) equatorial θ response to SH ETINMIP forcing. All panels are meridionally averaged from 5°S-5°N and temporally averaged from years 11-50. The 16°C isotherm from Ctrl is plotted as a solid white contour in all six panels and approximates the mean thermocline. Dotted white contours are the 16°C isotherm in the corresponding forced experiments.

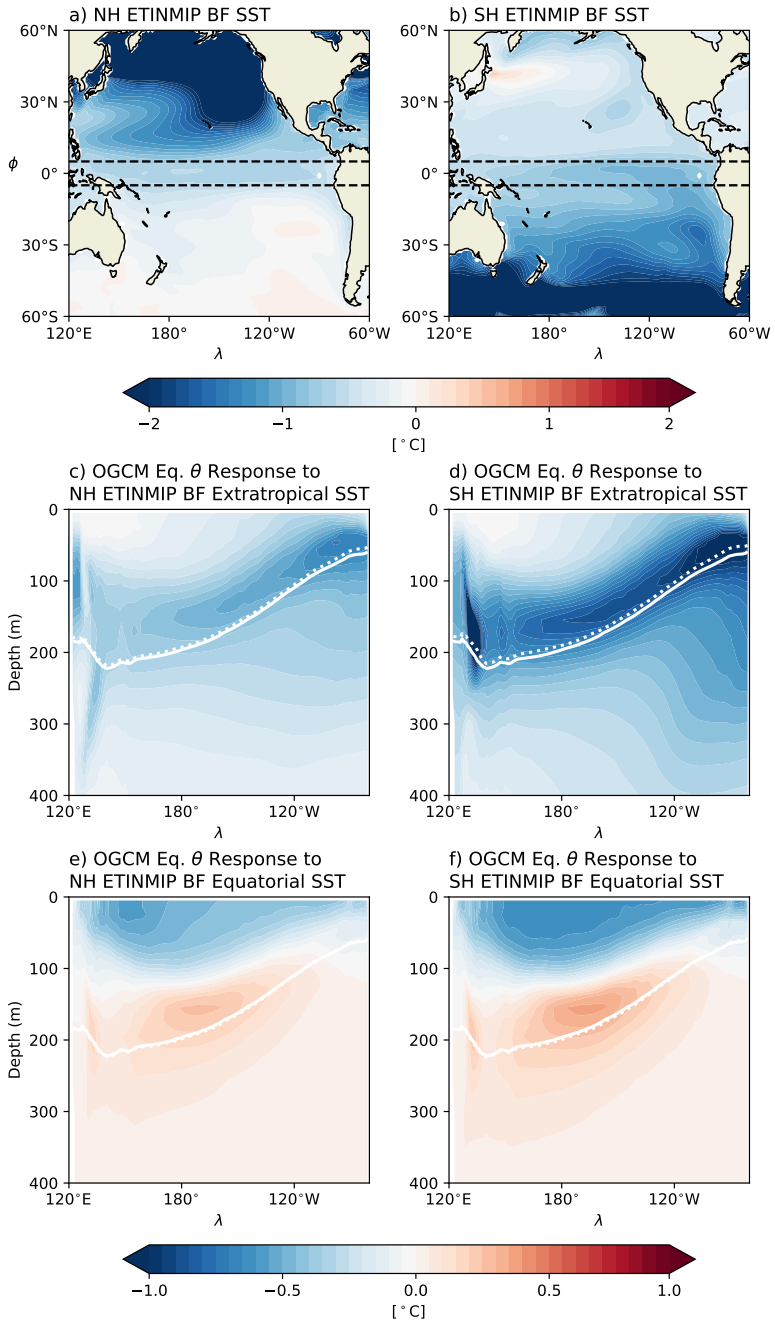

Figure S5. a) NH ETINMIP BF (Tau_1_S_NH-Tau1CO_2x1) SST pattern from CESM1. b) SH ETINMIP BF (Tau_1_S_SH-Tau1CO_2x1) SST pattern from CESM1. c) Equatorial θ response to remote NH ETINMIP BF SST forcing. d) Equatorial θ response to remote SH ETINMIP BF SST forcing. e) Equatorial θ response to local NH ETINMIP BF SST forcing. d) Equatorial θ response to local SH ETINMIP BF SST forcing. Dashed black lines in the top row correspond to the bounds that we separate the local and remote responses by. The 16°C isotherm in OCtrl (solid white contour in panels c-f) approximates the mean thermocline and the dashed white contour approximates the perturbed thermocline in respective forced simulations.